# Assessment of coastal inundation triggered by multiple drivers in Ca Mau Peninsula, Vietnam

Hung Nghia Nguyen<sup>1</sup>, Quan Quan Le<sup>1,2</sup>-, Dung Viet Viet Dung Nguyen<sup>1,3</sup>-, Hai Do Dac<sup>1</sup>, Hung Duc Pham<sup>4</sup>, Tan Hong Cao<sup>1</sup>, Toan Quang To<sup>1</sup>, Hai Do Dac<sup>1</sup>, Melissa Wood<sup>4</sup>Wood<sup>5,56</sup>, Ivan D. Haigh<sup>5</sup>-,

<sup>1</sup>Southern Institute of Water Resources Research, 658<sup>th</sup> Vo Van Kiet Avenue, District 5, Ho Chi Minh City, Vietnam <sup>2</sup>Geography and Environment, Loughborough University, Epinal Way, Loughborough, LE11 3TU, UK

<sup>3</sup>GFZ German Research Center for Geosciences, Section Hydrology, Potsdam 14473, Germany
 <sup>4</sup>Hydraulic Construction Institute, No. 3, Alley 95, Chua Boc Street, Trung Liet Ward, Dong Da District, Hanoi, Vietnam
 <sup>5</sup>School of Ocean and Earth Science, University of Southampton, Waterfront Campus, European Way, Southampton, SO14
 <sup>3</sup>ZH, UK

<sup>6</sup>Marine Systems Modelling Group, National Oceanography Centre, Joseph Proudman Building, 6 Brownlow Street,

15 Liverpool, L3 5DA, UK

Correspondence to: Hung Nghia Nguyen (hungsiwrr@gmail.com)

#### **Abstract**

The Ca Mau Peninsula Ca Mau Peninsula plays a critical role in the agricultural and aquaculture productivity of the Vietnam Mekong Delta (VMD), central to regional food security and the population's economic and social welfare. Unfortunately, this the region has also historically been a hotspot for been facing persistent threats from natural disasters, particularly from flooding, which is initiated caused by seasonal high flow from the river flux-upstream of the Mekong River and high tides. Climate change is expected and heightened sea levels downstream, but also to exacerbated the flooding in the future through rising sea levels, increased extreme rainfall, frequent tropical storm surges, by global climate change (e.g., increased rainfall and sea level rise, tropical storm surges) and human activities (e.g. river bed lowering, land subsidence) Human activities such as land subsidence, alteration of the riverbed and modifications of flood protection system can further complicate the situation. Quantification of The potential risks-hazards associated with these drivers is therefore rising inundation levels is important informationessential for shaping for the future sustainability of for the region and its ability to adapt to both current and forthcoming changes. Unfortunately, current research is limited, largely due to the lack of a quantitative coastal inundation map that incorporates both climate change and human impacts, hindering effective resilience and development planning. Without such a tool, planning for resilience and sustainable development is hindered The research around the influence of such drivers on future flood risk, in the Ca Mau Peninsula, is incomplete, primarily due to the absence of a quantitative coastal inundation map corresponding to future compounded scenarios. In this study, we therefore evaluate construct regional inundation maps and analyzing flooding dynamics in the Ca Mau pPeninsula using a fully calibrated 1D modellarge-scale hydrodynamic model set up for the whole VMD corresponding to several future scenarios. These scenarios are based on the individual drivers and their combinations, to representing a wide but plausible range of anthropogenic and climate changes compound scenarios. Our findings indicate that factors drivers such as increased high-flows upstream increases, alterations in the riverbed of the main Mekong channel, and occurrences of storm surges eaffecting the mainstream Mekong River, are unlikely to substantialsignificantly have minimum effects affect on the inundation dynamics in this the region. However, land subsidence, rising sea levels, and their combined effects emerge as the primary drivers behind the escalation of inundation events in both extent and intensity of the regional inundations the Ca Mau peninsula, both in terms of their extent and intensity, in the foreseeable future. These results results, hence, is expected to serve as vital groundwork for strategic development and investment as well as for emergency decision-making and flood management planning, providing essential insights for shaping development policies and devising investment strategies related to infrastructure systems in an area, which is this rapidly developing area.

**Keywords:** Ca Mau peninsula Ca Mau Peninsula, Mekong delta; flood hazard inundation risk, climate change, sea level rise, land subsidence; delta vulnerability; floods

# 1 Introduction

35

45

Deltas, home to over 500 million people globally, play a crucial role in can be important regions for agriculture and food production due to their fertile soils (Pont et al., 2002; Attaher et al., 2009; Edmonds et al., 2020). These low-lying regions, between river and coast, are highly susceptible to flooding, which can be further exacerbated by impacts of climate change (e.g. sea level rise, atmospheric changes), and human activities such as water abstraction (linked to land subsidence), river damming, and increased sand miningsand dredging rise (Syvitski et al., 2009; Giosan et al., 2014; Bevacqua et al., 2019; Best, 2019; Edmonds et al., 2020). According to current climate change projections, future flooding is expected to intensify in delta regions worldwide with coastlines facing heightened flood risks due to an increased frequency of extreme precipitation events and storm surges (IPCC, 2023). Previous research on delta flooding mainly examines individual flood drivers, such as riverine or tidal influences, with less focus on the compounded effects of multiple flood drivers occurring simultaneously. However, several studies -emphasize the significance of compound flooding, highlighting that the impact of simultaneous flood sources can exceed the sum of their individual effects

<u>Current research around delta flooding predominantly focuses on single drivers of flooding, from rivers or from the sea, with less emphasis on the combined hazard from multiple flood drivers occurring at the same time. Several studies underscore the importance of compound flooding, demonstrating that the impact of combined flood sources can surpass the sum of their</u>

individual effects (e.g., Leonard et al., 2014; Paprotny et al., 2018; Ward et al., 2018; Ward et al., 2018; Ward et al., 2018; Ganguli and Merz, 2019). For instance, Olbert et al., (2017) assess compound flooding in Cork City, Ireland, showing that while high sea levels alone may not cause flooding, they can worsen it when combined with river flooding utilized hydrodynamic modelling to assess compound flood mechanisms in Cork City, Ireland, considering tides, storm surges, river fluxes, and their interactions. The study revealed that while high sea levels alone may not induce flooding, their elevation can exacerbate flooding when coinciding with river flooding. Similarly, Leonard et al., (2014) showed an increasing inundation change when significant substantial river discharges coincided with extreme sea levels, compared to each source acting independently. Chen and Liu, (2014) used a hydrodynamic model to study flooding in the Tsengwen River basin, southern Taiwan, revealing that extreme storm surges and high upstream discharges together intensify flood severity more than either factor alone, employed a three dimensional hydrodynamic model to study inundation in the Tsengwen River basin, southern Taiwan, under the influence of storm surge, freshwater discharge, and their combination. Their findings indicated that the combination of extreme storm surge and high upstream river discharges could worsen flood severity compared to individual drivers. These studies highlight the importance of assessing future compound flooding for effective planning, risk management, and mitigation. A comprehensive understanding of current and future flood hazards allows for the implementation of engineering solutions to reduce fatalities, infrastructure challenges, environmental damage, and societal impacts (Leonard et al., 2014; Haigh et al., 2014; Wahl et al., 2018; Ward et al., 2018; Paprotny et al., 2018; Edmonds et al., 2020), while optimizing flood protection and levee systems Moreover, at the emergency planning level, it is essential to consider the impacts of compound flooding to optimize flood protection infrastructure and levee systems (Leonard et al., 2014, Ward et al., 2018).

70

80

85

These studies underscore the crucial necessity of assessing the future implications of compound flooding for emergency decision making, flood management, and planning. It is imperative to accurately estimate and quantify compound flood risk, to facilitate proactive mitigation and adaptation measures. A comprehensive understanding of both current and anticipated combined flood hazards enables the implementation of effective engineering solutions, appropriately budgeted to mitigate flood related fatalities, operation and construction of technical infrastructure, environmental degradation, and societal impacts (Leonard et al., 2014; Haigh et al., 2014; Wahl et al., 2018; Ward et al., 2018; Paprotny et al., 2018; Edmonds et al., 2020). Moreover, at the emergency planning level, it is essential to consider the impacts of compound flooding to optimize flood protection infrastructure and levee systems (Leonard et al., 2014, Ward et al., 2018).

For the Vietnam Mekong delta (VMD), <u>eurrent previous</u> research provides insight into the present challenges that exacerbate flood risk in the region. <u>Recent river damming and sand mining in the VMD have considerably lowered the riverbed, raising concerns about their impact on the hydraulic regime Recently, river damming and sand mining has resulted in lowering of the riverbed in the VMD (Kummu et al., 2010; Bravard et al., 2013; Lu et al., 2014; Bravard et al., 2013; Hackney et al., 2021). It</u>

is a major concern because of its potential to affect the hydraulic regime. For instance, Vasilopoulos et al., (2021) estimated that two principal channels of the Mekong delta (the Mekong and Bassac Rivers) experienced riverbed lowering of an average of 2.5 m ( $\sigma$  = 3.9 m) between 1998 and 2018, which heightened tidal inundation risk (Vasilopoulos et al., 2021; Riverbed lowering also directly impacts the extent of tidal intrusion penetrating inland, potentially contributing to greater tidal inundation risk (Eslami et al., 2019) Eslami et al., 2019). -Within the broader VMD area, the average vertical sinking of land is a recent phenomenon now occurring at rates approximately around 0.03 m per year (Erban et al., 2014). This subsidence is expedited by the extraction of groundwater linked to agricultural practices and the expanding population within the delta (Erban et al., 2014; Minderhoud et al., 2020). For the future VMD, the IPCC report report of IPCC, (2007) considers that the VMD will be one of the zones that will be most affected by climate change (IPCC, 2007), with SSP5-8.5 (very high emissions scenarios) projections suggesting a sea level rise of up to approximately 1 m by the end of the century by the end of this century. (Fox-Kemper et al., B., Hewitt, H. T., Xiao, C., Aðalgeirsdóttir, G., Dri jfhout, S. S., Edwards, T. L., Golledge, N. R., Hemer, M., Kopp, R. E., Krinner, G., Mix, A., Notz, D., Nowicki, S., Nurhati, I. S., Ruiz, L., Sallée, J. B., Slangen, A. B. A., and Yu 2021) NASA, (2021) suggest that under scenario SSP5-8.5, the VMD could experience a mean sea level rise (SLR) of 1 m by the end of the century, potentially increasing flood magnitudes. This level of sea level rise could contributing to the threat of greater flood magnitudes for the region (Västilä et al., 2010; Lauri et al., 2012; Hoang et al., 2016; Tran et al., 2016; MONRE, 2016; Minderhoud et al., 2019). For example, a projected 0.8 m rise in mean sea level could submerge approximately 51% of the VMD plain (According to Minderhoud et al., (2019), approximately 51% of the VMD plain would be submerged if the mean sea level rose by 0.8 m. Wood et al., (2023) highlighted a significant uptick in extreme storm surges anticipated to this coastline by year 2050, linked to the heightened occurrence of intense tropical cyclones. Van et al., (2012) used 1D modelling to study the impacts of climate change on future flood risk and showed the downstream area of VMD inundation will be more aggravated in terms of higher magnitude and longer flooding durations because of the compounding effects of increasing high tide and fluvial floods. Triet et al., (2020), used a quasi two dimensional hydrodynamic model to estimate the future flood regime of VMD. They found that SLR and land subsidence would present the highest impact driving flooding in the VMD, with flooded areas extended by around 20 27% in the future period (2036 2065) compared to the past period 1971 2000. Furthermore, Wood et al., (2023) highlighted a substantial uptick in extreme storm surges anticipated to this coastline by year 2050, linked to the heightened occurrence of intense tropical cyclones.

100

105

110

115

120

125

Despite the valuable insights from aforementioned studies (Van et al., 2012; Hoang et al., 2016; Duc Tran et al., 2018; Triet et al., 2020), attention has not yet been focused on the Ca Mau Peninsula (CMP), the most flood-prone coastal region within the VMD, where the local population faces recurrent flooding events Despite these significant findings, prior research has yet to direct attention to the Ca Mau Peninsula, an area within the Mekong Delta that stands as the most susceptible region (see Fig. 2a-1a for exact locations). —Moreover, these studies use bathymetric data from various sources, which may lead to inconsistencies and errors when merged, and are potentially outdated due to substantial anthropogenic-induced riverbed

lowering in the VMD (Bravard et al., 2013; Vasilopoulos et al., 2021). Additionally, while these studies focus on water level estimations within river channels, they fail to address inundation in surrounding areas and do not consider the potential rise in storm surge frequency in the Mekong region due to projected climate change.

Therefore, our study aims to comprehensively assess the compound flooding dynamics of the coastal areas of the CMP, a region increasingly vulnerable to a variety of environmental and human-driven changes. We specifically focus on understanding how shifts in key factors, such as storm surges, sea level rise, river discharge, land subsidence, human-induced riverbed lowering, interact to trigger flooding events. By providing a more detailed understanding of the interactions between natural and anthropogenic forces, we aim to offer actionable insights that can enhance flood preparedness, foster resilient infrastructure, and support adaptive regional planning. In doing so, we strive to help mitigate flood hazards and contribute to long-term sustainability in the CMP. Furthermore, prior research has used bathymetry data collected from a range of sources (introducing inconsistencies and possible errors in merging datasets), which are now potentially out of date considering the scale of anthropogenic riverbed lowering in the VMD. They also do not incorporate the potential for increased frequency of storm surges in the Bassac River region, as a consequence of projected climate change.

Future planning, based on projections, will include water control systems, expressways, coastal embankments to manage tidal surges in the West and East Seas, and saltwater control gates along the Bassac River. These measures are crucial for relevant authorities, such as the Ministry of Natural Resources and Environment (MONRE), the Ministry of Transport (MOT), the Ministry of Construction (MOC), the Ministry of Agriculture and Rural Development (MARD), and the Ministry of Planning and Investment (MPI), in making informed, long-term development decisions relevant. Successful implementation will enhance the region's flood resilience and foster sustainable growth in the face of climate change. Therefore, our study aims at assessing compound flooding dynamics of the coastal environs of the Ca Mau Peninsula. Our focus lies in assessing potential shifts in the diverse factors that serve as triggers for flooding events in this region. Recognizing the profound significance of this inquiry, particularly concerning the heightened vulnerability of local communities to flooding, our overarching aim is to refine decision making frameworks, enhance flood management strategies, and bolster regional planning initiatives. Through a nuanced exploration of both natural phenomena and anthropogenic influences, we seek to furnish nuanced insights capable of informing proactive measures aimed at mitigating flood hazards. Our ultimate aspiration is to engender greater resilience among the populace inhabiting the Ca Mau Peninsula in the face of recurrent flood occurrences. Therefore, this article represents an important contribution for analysis, forecasting, warning, and proposing various flood control solutions for the Ca Mau region. Based on future predictions, water control systems and future developments will be planned, including expressways, coastal embankments to control tidal surges in the West Sea, East Sea, and saltwater control gates along the Hau River. The article aims to achieve the following objectives:

The article aims to achieve the following objectives:

130

135

140

145

150

- Develop a set of flooding calculation tools for the Ca Mau Peninsula CMP with a higher level of detail than existing tools to support long-term research and development for the region;
  - Analyse in detail for the first time the causes of compound flooding on the <u>Ca Mau PeninsulaCMP</u>, quantifying the
    impact of each cause and compound factors based on hydraulic models. The study examined both present and future
    scenarios, encompassing variations in upstream freshwater flow, human-induced riverbed lowering, land subsidence,
    and eustatic sea-level rise; and
  - Establish and compare the levels of inundation change in the study area, serving as a basis and direction for the
    construction and development of infrastructure to protect residents, transportation (expressways, internal routes), and
    the distribution of more effective industrial clusters and wider VMD zones.



170 Figure 1. The extensive flooding within Ca Mau city (see Fig. 2a for exact location), resulting from intense rainfall and elevated tides on October 2, 2023 (source: thanhnien.vn)

#### 2 Study Area, Flood Model and Methods

#### 2.1 Study area

175

180

165

The Ca Mau Peninsula Ca Mau Peninsula (CMP), located in the southern coastal region of the VMD, covers an area of about 5,210 km² and is\_currentlyeurrent inhabited by 1.19 million people (General Statistics Office of Vietnam, 2020) (Figure. 2a1a). In 2020, the aquaculture sector in the CMP expanded to 285.5 thousand hectares, representing 37.16% of the Mekong Delta's aquaculture area and 26.49% of the nation's total. In 2020, the aquaculture sector in the Ca Mau Peninsula expanded to cover an area of 285.5 thousand hectares. This constituted 37.16% of the aquaculture area within the Mekong Delta region and 26.49% of the nation's total aquaculture area. The total fishery output reached 590,191 tons, contributing to 12.2% and 6.8% of the fishery output within the VMD and the entire nation, respectively (General Statistics Office of Vietnam, 2020). Furthermore, the CMP, home to 77% of the mangrove forests in the VMD region, plays a crucial role in managing, conserving, and promoting the sustainable development of the Mui Ca Mau Biosphere Reserve (Tinh et al., 2009; Son et al., 2015; Thuy et al., 2020). It is recognized as one of the country's top geographical, cultural, and ecological landmarks, with its unique river mouth and coastal ecosystems.

In addition, with a rich mangrove ecosystem that covers 77% of the mangrove forests in the VMD region, the Ca Mau Peninsula holds a pivotal role in overseeing, preserving, and fostering the sustainable development of the Mui Ca Mau Biosphere Reserve (Tinh et al., 2009; Son et al., 2015; Thuy et al., 2020). It stands out as one of the nation's premier geographical, cultural, and ecological attractions, characterized by its distinctive river mouth and coastal ecosystems.

The hydro-climate in the broader VMD region is tropical, with its hydrology heavily-influenced by a monsoon seasonal flood-pulse, marked by distinct dry and flood seasons\_(MRC\_2005). The flood season typically spans from mid-May to October, representing over 90% of the annual precipitation in the VMD (Kingston et al., 2011), and accounts for 80-90% of the total annual river flows (Triet et al., 2017). The Ca Mau PeninsulaCMP is a low-lying area that is frequently flooded. Its average elevation ranges from 0.5-2 m to 1.5 m above mean sea level (Karlsrud et al., 2020; (Tran et al., 2024), with a coastline length of 254 km with 154 km bordering 154 km the Gulf of Thailand in the west and 100 km facing 100 km the East Sea in the east -(The People's Committee of Ca Mau Province, Province 2023). In the East Sea, a semi-diurnal tidal pattern with an amplitude ranging from 2.5 to 4.0 m is observed, whereas the Gulf of Thailand experiences a diurnal tidal regime with amplitudes varying from 0.8 m to 1.2 m (Gugliotta et al., 2017). This region is characterized by a dense network of natural and human-made rivers, canals and is currently undergoing infrastructure development, including expressways, coastal embankments, and water control works along the West Sea and East Sea coasts (The People's Committee of Ca Mau Province, 2023).

### 2.2 Flood model

190

195

200

205

210

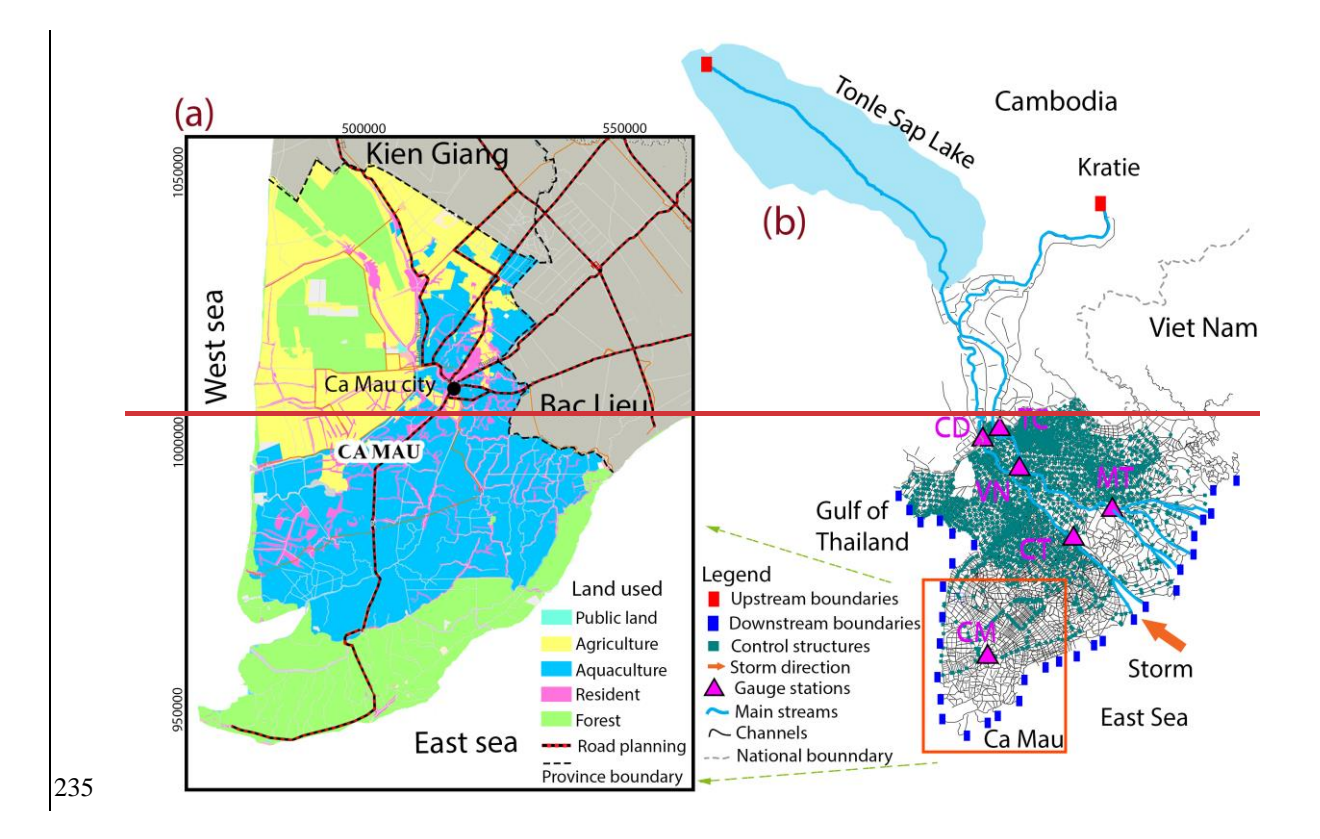
We utilized a one-dimensional (1D) hydrodynamic model covering the entire Mekong Delta, extending from Kratie, Cambodia to the coastal zone in Vietnam. -The model was initially developed by Dung, (2011) Dung et al., (2011) using the modelling package MIKE11-HD developed by the Danish Hydraulic Institute (DHI). It was set up to represent the complex river network and floodplains and numerous flood control structures (e.g dikes, sluice gates) in the VMD (Fig. 2b1b). The model includes approximately 4,235 river branches and 564 floodplain compartments across the VMD, with secondary channel data in the CMP having a resolution ranging from 1 km to 3 km per channel. The model utilizes the WGS84 coordinate system, with elevations referenced to the Hon Dau Mean Sea Level. For the Mekong River's main channels and the Tonle Sap Lake system, topographic data were compiled and updated through various projects of varying accuracy (Dung et al., 2011). The representation of floodplains differs between regions due to their unique characteristics. In the Cambodian Mekong Delta, where floodplains lack significant channelization and dike infrastructure, they are represented as channels with broad cross-sections. (Dung et al., 2011). Conversely, in the VMD, the floodplains are highly compartmentalized into numerous flood cells to safeguard agricultural activities. These cells are depicted as wide cross-section channels enclosed by dikes.

This 1D-hydrodynamic modeling approach, with its detailed floodplain representation, is justified as a practical and efficient solution for capturing the essential hydrodynamic processes within the model domain. Additionally, by incorporating a quasi-2D representation of the floodplains, it strikes a balance between the oversimplicity of non-hydrodynamic and purely

1D approaches, and the highly computational demands of fully 2D models. More details on the model development can be found in Dung, (2011).

# Dung et al. (2011a, 2011b).

The main input boundary is the daily discharge data at Kratie, supplied by the Mekong River Commission (MRC: 220 https://portal.mrcmekong.org/monitoring/river-monitoring-telemetry). Hourly tidal stage measurements from coastal stations along the VMD coastline are used to establish the downstream boundary conditions, provided by the Southern Regional Hydro-Meteorological Center (SRHMC) (Fig. 1b), The primary input boundary is the daily discharge at Kratie, Tidal stage measurements from coastal stations along the VMD coastal area are utilized to define downstream boundary conditions. The model uses approximately 30,000 computational nodes across the domain and operates with a 5-minute time step to ensure stability and enable accurate, dynamic simulations of hydrodynamic processes. The model utilises around 30,000 225 computational nodes around the domain. Simulated water levels are also output hourly and referenced to the Hon Dau mean sea level. A key contribution of this study is the updating of datasets to be fed into the modelling. This includes updating dvke heights throughout the VMD, from data provided by Southern Institute of Water Resources Research (SIWRR) (surveys carried out 2018-2019). Additionally, the tidal and saline prevention culvert systems along the wWestern coastal of VMD have 230 been updated up to 2019. Riverbed topography data for the mainstream of the Mekong River within VMD was updated in 2018, adopted from Vasilopoulos et al., (2021).



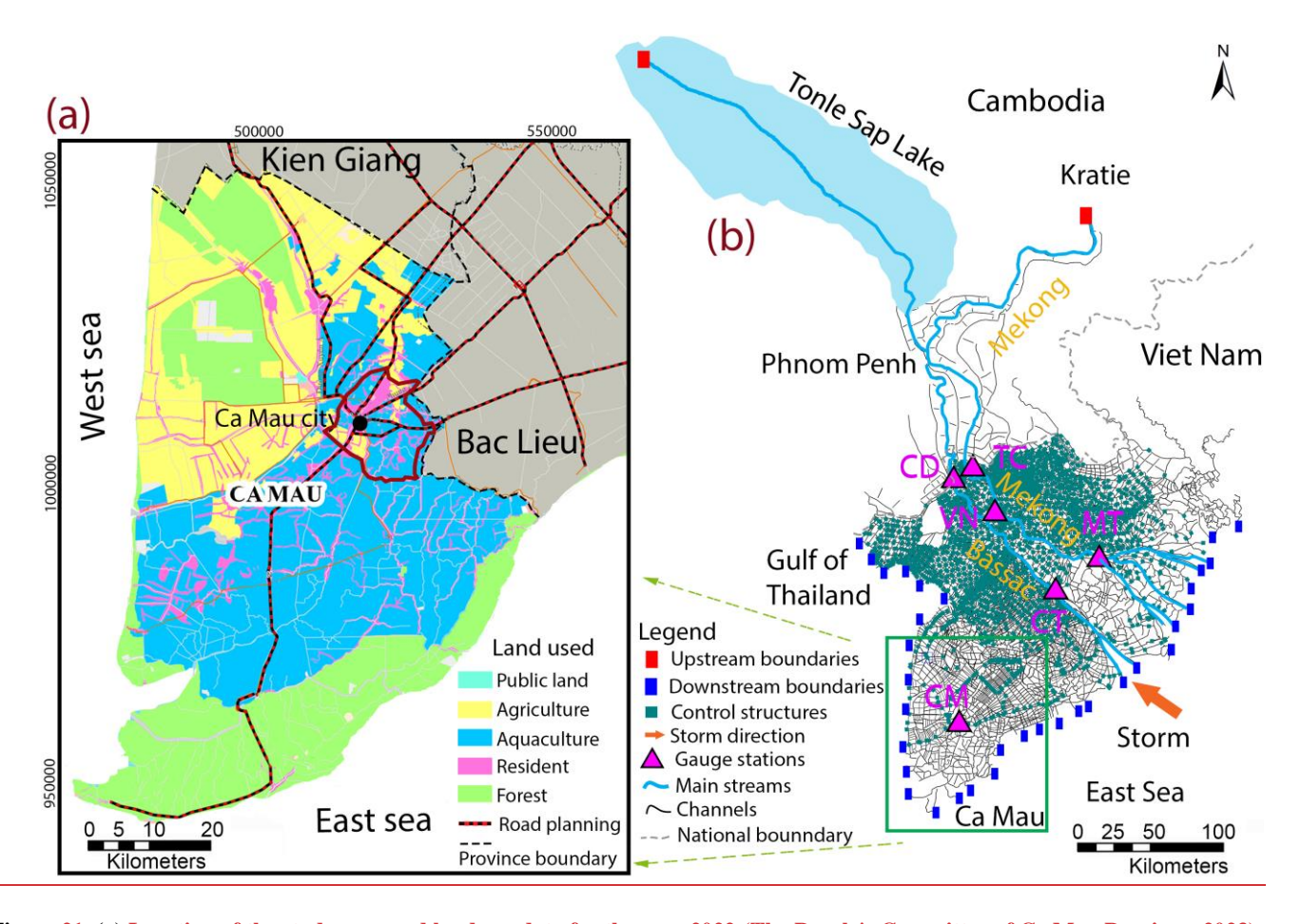


Figure 21. (a) Location of the study area and land use data for the year 2022 (The People's Committee of Ca Mau Province, 2023); (b) the 1D model used in this study The study area's location and the land use for the year 2022, along with the projected road infrastructure development in the study area up to 2030; (b) the 1D model used in this study

A key contribution of this study is the updating of datasets to be fed into the modelling. This includes updating dyke heights throughout the VMD, from data provided by Southern institute of water resource research (SIWRR) (surveys carried out 2018-2019). Additionally, the tidal and saline prevention culvert systems along the Western coastal of VMD have been updated up to 2019. Riverbed topography data for the mainstream of the Mckong River within VMD was updated in 2018, based on the study of (Vasilopoulos et al., 2021). This bathymetry data was incorporated at approximately 3 km intervals along the entire Mekong and Bassac channels. The study utilises hydrological data pertaining to water discharge and water level, gathered from various stations situated across the primary channels of the VMD (Table 1). The dataset comprises a single set of long-term daily water flow data at Katie, obtained from the Mekong River Commission (MRC). Other data, including water discharge and water level in the mainstream Mekong River, are recorded on an hourly basis. Additionally, daily maximum and minimum water levels within the study area have been collected. These measurements are obtained from gauges operated by the Southern Regional Hydro Meteorological Center (SRHMC) and are referenced to the Hon Dau Mean Sea Level (MSL)

datum. The specific locations and names of each station can be found in Table 1 and Figure 2. A Digital Elevation Model (DEM) for the Ca Mau peninsula CMP, has been acquired from the Ministry of Natural Resources and Environment (MONRE) in 2008 for the purpose of creating inundation maps (Tran et al., 2016) -(Appendix A, Fig. A1). This DEM utilizes the WGS84 coordinate system and is based on the Hon Dau meanmeans sea level vertical datum, featuring a resolution of 5 m x 5 m. The DEM is using survey points and the topographical maps with the elevation points and contour lines, which were obtained from geodetic survey and photogrammetric data. Terrain data are aggregated and selected from topographic maps of the largest scale and best quality (T. Tran et al., 2016). The DEM is considered as the best elevation data currently available for the VMD, and it was used for the inundation in VMD under projection of future sea level rise in Vietnam (Tran et al., 2016) as well as other study (Vu et al., 2021; (Dang et al., Reid, and Kumar 2023).

260

265

270

275

280

255

#### Table 1. Information on Cauge Stations and data availability

#### 2.3 Model calibration and validation

To assess the precision of the updated model, it was subjected to testing under different hydraulic upstream conditions. Specifically, tThe updated model has been re-calibrated using observed data from the high-water flux event in 2018, with a water volume of 454 billion m<sup>3</sup> at Kratie (Fig. 32). In comparison, the annual water volume at Kratie from 2000 to 2021 averaged at 390 billion m<sup>3</sup>. The 2018 hydraulic year had annual volume exceedance frequency is approximately 20%, relative to the 2000-2021 data range. Following this, the model's validation was carried out using data from the year 2016, which was linked to a low-water flux event, where the water volume amounted to 331 billion m<sup>3</sup> (Fig. 32), -During this period, the annual volume exceedance frequency was approximately 78%, compared to the historical data range spanning from 2000 to 2021. The choice of these particular years was based on their close alignment with the observed bathymetry used in the model, signifying minimal changes in the riverbed. As a result, the model underwent calibration for a high flood event, and validation against a low flood event, enabling an evaluation of the model's suitability across a broad range of potential flood magnitudes. For the calibration and validation processes, the model is driven by observed daily upstream water discharge (m<sup>3</sup>s<sup>-1</sup>) values at Kratie, while downstream boundaries are influenced by observed hourly tidal stages along the Mekong coastal zone for the years 2018 and 2016, respectively. The calibration and validation procedures involved using observed upstream water discharge values at Kratie gauges, recorded on a daily basis. Additionally, downstream boundary conditions were determined based on hourly tidal stage measurements taken along the Mekong coastal zone for the years 2018 and 2016, respectively. The calibration and validation compared hourly simulated and observed water levels and discharge at various stations located across the primary channels of the VMD and the maximum water within the Ca Mau region (see Table 1 and Fig. 1b for specific locations). These measurements were provided by SRHMC, and were made available through SIWRR.

The calibration procedure entailed fine-tuning of the Manning roughness parameters, a standard practice in hydraulic models. The initial roughness values were based on Manh et al., (2014), who categorized the model domain into distinct zones, assigning specific Manning's n values to each zone to represent their unique hydraulic characteristics. These values were systematically refined to achieve the best agreement between the model's predicted water levels and discharges and the observed data. Specifically, the calibration process utilized monitoring stations located along the main Mekong channel in Vietnam (Fig. 1b, Table 1). Model outputs were compared with observed water levels and discharges, and any discrepancies prompted adjustments to the zone-specific roughness values (Fig. 3 and Table 2). The model was iteratively rerun until optimal results were achieved. The final calibrated Manning's n values are detailed in Table 3. A comprehensive result and discussion of the calibration and validation procedures follow in the next paragraph.

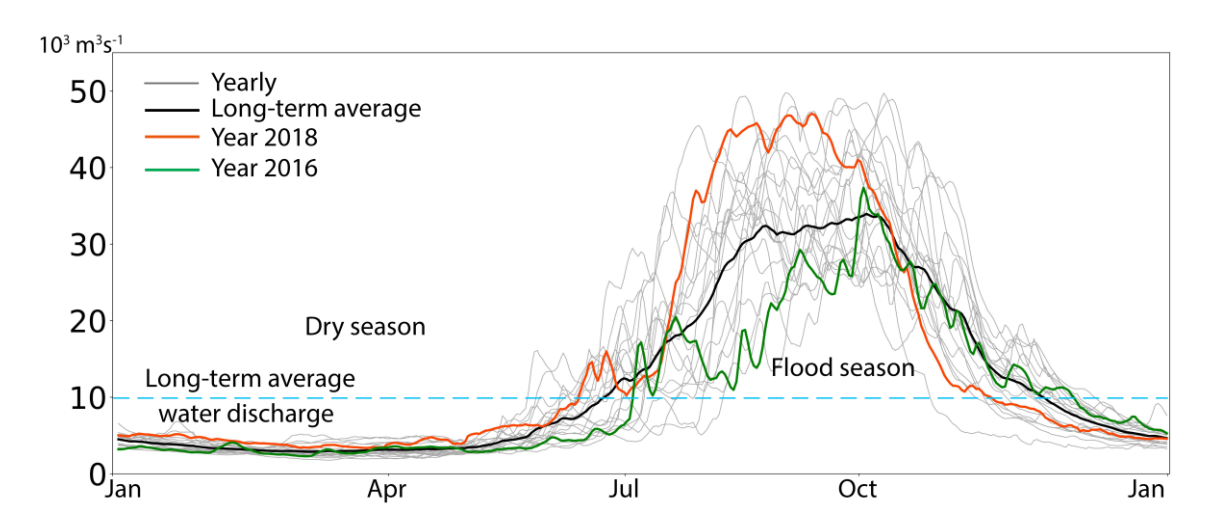


Figure 32. The daily discharge at Kratie was utilized as the upstream boundary for the modelling scenarios, which including the daily long-term average water discharge spanning from 2000 to 2021 and the observed water discharge for the year 2018 and 2016

### Table 1. Information on Gauge Stations and data availability

285

290

NI.	C ( d-)	T -444 J - (0NT)	T 24 1 - (0T)	Available o	lata period	Resolution	Channel
No	Gauges (code)	<u>Latitude (<sup>0</sup>N)</u>	Longitude ( <sup>0</sup> E)	<u>Discharge</u>	Water level	_	_
1	Kraite (KH_014901)	12.481	<u>106.018</u>	<u>2000-2021</u>	<u>1933-2022</u>	<u>Daily</u>	Mekong
2	Tan Chau (TC)	10.801	105.248	<u>2016-2018</u>	<u>2016-2018</u>	<u>Hourly</u>	Mekong
<u>3</u>	Vam Nao (VN)	10.417	<u>105.644</u>	<u>2016-2018</u>	<u>2016-2018</u>	<u>Hourly</u>	Mekong
<u>4</u>	My Thuan (MT)	10.275	<u>105.926</u>	<u>2016-2018</u>	<u>2016-2018</u>	<u>Hourly</u>	Mekong
<u>5</u>	Chau Doc (CD)	10.705	<u>105.134</u>	<u>2016-2018</u>	<u>2016-2018</u>	<u>Hourly</u>	<u>Bassac</u>
<u>6</u>	Can Tho (CT)	10.053	<u>105.787</u>	<u>2016-2018</u>	<u>2016-2018</u>	<u>Hourly</u>	<u>Bassac</u>
<u>7</u>	Ca Mau (CM)	9.176	105.155	Ξ	<u>2016-2018</u>	<u>Daily</u>	Ganh Hao

The calibration procedure entailed fine-tuning of the Manning roughness parameters, a standard practice in hydraulic models. This process utilized monitoring stations for water discharge and water levels positioned along the primary Mekong channel in Vietnam (Fig. 2b and Table 1). The model's predictions were extracted and compared with the corresponding observed data. In cases where the model's performance was deemed unsatisfactory, adjustments were made to the roughness coefficient in those specific zones. The model was then rerun through multiple iterations until optimal results were achieved.

300

305

The Nash-Sutcliffe model efficiency coefficient (NSE) (Nash and Sutcliffe, 1970), as specified in Eq. (1), along with the coefficient of determination ( $R^2$ ), as defined in Eq. (2), which indicates the proportion of variance in both simulated and observed data explained by the model (Moriasi et al., 2007) was utilized to assess the accuracy of the comparison between the recently calibrated predictions and the observed data (Nash and Sutcliffe, 1970).

$$NSE = 1 - \frac{\sum_{t=1}^{T} (x_{tn}^{t} - x_{0}^{t})^{2}}{\sum_{t=1}^{T} (x_{t}^{t} - \overline{x_{0}})^{2}}$$
(1)

$$R^{2} = \frac{\left[\sum_{t=1}^{T} (X_{m}^{t} - \overline{X_{m}})(X_{0}^{t} - \overline{X_{0}})\right]^{2}}{\sum_{t=1}^{T} (X_{m}^{t} - \overline{X_{m}})^{2} \sum_{t=1}^{T} (X_{0}^{t} - \overline{X_{0}})^{2}}$$
(2)

In this equation,  $\bar{X}_0$  represents the mean of observed values and  $X_0^t$  is the observed hourly data at time t (from 1 to T).  $\bar{X}_m$  represents the mean of calibrated simulated value,  $X_m^t$  is the hourly calibrated value at time t, and  $X_0^t$  is the observed data at time t. Generally, NSE values below 0.5 indicate suboptimal calibration performance, while NSE values surpassing 0.5 suggest a satisfactory model performance. NSE values exceeding 0.65 indicate a well-performing calibration, and values surpassing 0.8 indicate a highly accurate calibration (Ritter and Muñoz-carpena, 2013).  $R^2$  ranges from 0 to 1, with higher values indicating less error variance (Moriasi et al., 2007).

The model is run for both dry low-flow periodsseasons, characterized by water discharge falling below the long-term average values spanning from 2000 to 2021, and flood seasons, identified by days when water discharge surpasses the average values within the same dataset. These definitions align with those outlined by the MRC, (2011).— In the calibration process of inundation within the Ca Mau peninsulaCMP, the deviation value is utilized to assess the accuracy between the modelled and observed data. The water level at the Ca Mau station, situated in the central part of the study area, serves as the basis for this assessment. The deviation value was also calculated, as specified in Eq. (2).

$$Dev = \left| \frac{obs - sim}{obs} \right| *100\% \tag{2}$$

where *Sim* is the simulated maximum water level value and *Obs* is corresponding observed data. The best performant has a *Dev* of 0.

Calibration establishes the most appropriate Manning coefficient (n) -values for the model (see Table 3). In the subsequent validation phase, the model was tested using data from the different hydraulic year of 2016.

In the calibration step, the results demonstrate outstanding consistency between the simulated and observed water levels and water discharge throughout the simulation period and across the entire spatial extent of the VMD (Fig. 4a3a). The average NSE values for these measurement points exceed 0.8, with the exception of the Vam Nao station, which NSE for discharge calibration registered at 0.63. This suggests the effective performance of the model (Table 2). The results also emphasizes that the agreement between the predicted water levels and the corresponding observed values tends to be higher than that for water discharge across all gauging stations. While there is generally good agreement between the predicted and observed maximum water levels, it's noteworthy that the observed maximum water level tends to be slightly higher than the corresponding value at the Can Tho station. The simulated maximum water level at the Ca Mau gaging station was extracted and compared with the observed data. The results indicate that, during the calibration phase, the simulated maximum water level was approximately 0.92 m, compared to the observed value of 0.84 m, resulting in a deviation (Dev) of 10%, indicating a satisfactory level of agreement. For the validation stage, the results reveal a consistently strong agreement between the simulated outcomes and the corresponding observed data across the VMD gauging stations (Fig. 3b and Table 2). There is a persistent pattern of high agreement in water level values and an overall strong agreement in terms of water discharge. At the Ca Mau gauging station, the simulated maximum water level was 0.86 m, while the observed value was 0.77 m, yielding a Dev of 12%. This deviation implies a reasonably good agreement between the simulated values and the observed data.

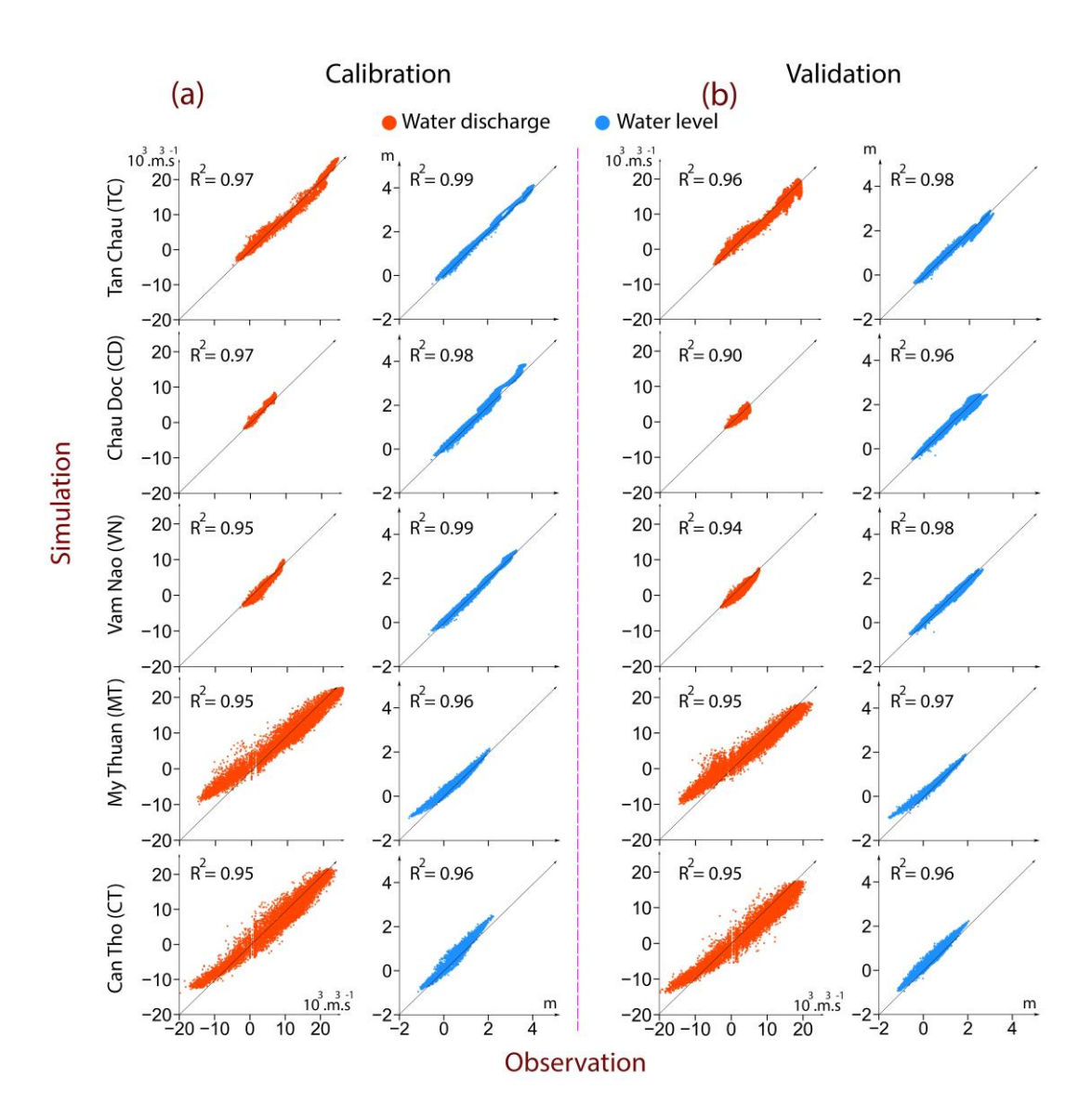


Figure 43. Assessing the agreement between the predicted and observed hourly data for water level and water discharge at monitoring stations throughout the VMD during the calibration run in 2018 and validation run in 2016 - along with the coefficient of determination (R<sup>2</sup>).

Table 2. The NSE coefficient was calculated across a range of river gauge stations spanning the VMD, averaging the values for distinct dry and flood season periods during the calibration and validation steps

		<u>Calib</u>	<u>ration</u>		<u>Validation</u>				
<u>No</u>	Water level (WL)		Water discharge (Q)		Water leve	<u>el (WL)</u>	Water discharge (Q)		
	<u>Dry</u>	Flood	<u>Dry</u>	Flood	<u>Dry</u>	Flood	<u>Dry</u>	Flood	
Tan Chau	0.90	0.97	0.94	0.93	0.95	0.98	0.91	<u>0.87</u>	
Chau Doc	<u>0.96</u>	0.94	0.92	0.93	0.98	0.94	0.87	<u>0.79</u>	
Vam Nao	0.97	0.97	0.63	0.83	0.98	0.97	0.73	0.68	
My Thuan	0.98	0.97	0.93	0.93	0.95	0.98	0.91	0.87	
Can Tho	0.88	0.88	0.95	0.94	0.98	0.94	0.87	<u>0.79</u>	

Table 3. The Manning roughness coefficient (n) is categorized based on different zones using in the modelling. The Manning roughness in the channel changing for different cross-sections within the same zone

Zone	<u>Description</u>	Manning's coefficient (n)
1	Mekong River: Kratie to Phnom Penh	0.032
<u>2</u>	Mekong River: Phnom Penh to Tan Chau	0.032 to 0.027
<u>3</u>	Mekong River: Tan Chau to My Thuan	0.027 to 0.025
<u>4</u>	Mekong River: My Thuan to River months	0.025 to 0.016
<u>5</u>	Bassac River: Phnom Penh to Chau Doc	0.032
<u>6</u>	Bassac River: Chau Doc to Can Tho	0.032 to 0.025
<u>7</u>	Bassac River: Can Tho to River months	0.025 to 0.017
<u>8</u>	Side channels	0.033
<u>9</u>	Floodplain	0.033

For the validation stage, the results reveal a consistently strong agreement between the simulated outcomes and the corresponding observed data across the VMD gauging stations (Fig. 4b and Table 3). There is a persistent pattern of high agreement in water level values and an overall strong agreement in terms of water discharge. At the Ca Mau gauging station, the simulated maximum water level was 0.86 m, while the observed value was 0.77 m, yielding a *Dev* of 12%. This deviation implies a reasonably good agreement between the simulated values and the observed data.

370

365

Table 3. The NSE coefficient was calculated across a range of gauge stations spanning the VMD, averaging the values for distinct dry and flood season periods during the validation step

By integrating 2018 riverbed bathymetry data and 2019 infrastructure information within the VMD, the calibration and validation results reveal that the updated flood model performs well in capturing flood dynamics across the VMD, showcasing the model's ability to effectively simulate diverse hydraulic conditions. The calibration and validation results reveal that the updated flood model is performing well in capturing flood dynamics across the VMD. By integrating 2018 riverbed bathymetry data and 2019 infrastructure information, particularly in the main river system, we've significantly improved the model's accuracy. Calibration for the high water year of 2018 and validation for the low water volume year of 2016 have yielded highly reliable results, showcasing the model's ability to simulate diverse hydraulic conditions effectively. Consequently, this model will be utilized to comprehensively investigate the flooding regime in the VMD through various simulation scenarios.

# 2.4 Simulation Scenarios Scenarios

In order to assess the potential future inundation across the study area, a range of scenarios involving variations in upstream freshwater flow, human-induced riverbed lowering, land subsidence, <a href="mailto:sectors below">sStorm surge</a> and eustatic sea-level rise were introduced into the modelling process for analysis. The details of each scenario are outlined in Table 4 and are discussed in more detail in the sub-sections below.

## 2.4.1 Individual drivers

First, we ran a Baseline Scenario (S0). This simulation uses the daily time series of long-term mean flow at Kratie ( $Q_M$ ) spanning from 2000 to 2021 (Fig. 32), where the water volume at Kratie is approximately 390 billion m<sup>3</sup> and the downstream boundary conditions were determined using hourly observed tidal stage measurements taken along the Mekong coastal zone

for the year 2018. This scenario serves as the foundation for modelling average flooding in the Ca Mau Peninsula CMP and is employed for comparison with alternative flood scenarios.

We then ran 7 other scenarios, varying the upstream discharge, storm surge, lowering the riverbed, accounting for land subsidence and sea level rise, as described below.

High upstream flow **(S1)**: The observed water discharge at Kratie for the 2018 vear  $(Q_{20\%})$  was employed as the upstream water discharge, which involved a water volume estimated at around 454 billion m<sup>3</sup> and the total volume exceedance frequency is approximately 20% within the historical data range from 2000 to 2021. This scenario is utilized to evaluate inundation in the study areas under high water upstream flux.

400

405

410

415

420

**Storm surge** (S2): This scenario assesses the impact of storm surge inundation, caused by tropical cyclone, in the Ca Mau PeninsulaCMP. The chosen location for the scenario's storm surge impact is the Bassac channel mouth along the VMD coastal area (Fig. 1b). This selection is based on the Bassac River being the primary stream in the VMD, capable of transmitting storm surge impacts further inland and its close proximity to the study area. This selection is based on the significance of the Bassac River as the primary stream in the VMD, capable of transferring the storm surge impact further inland. Additionally, this channel is in close proximity to the study area. Information on the tropical cyclone annual exceedance probability of 1% AEP ( $TC_{1\%}$ ) affecting the VMD at the Bassac River mouths, has been utilized for this scenario. The timing of the tropical cyclone occurrence was chosen in the middle of September, coinciding with the period when flooding caused by high upstream water discharge typically takes place. The rise in water level due to the tropical cyclone impacting the VMD at the Bassac River mouth has been synchronized with a full tidal cycle in the VMD coastal zone at the time of the storm, serving as the downstream boundaries. This integration results in the maximum water level at the Bassac River mouth boundary rising up to 2.9 m during the storm. These storm surge data for the VMD coastal zone has been adopted from Wood et al., (2023).

Human-induced riverbed lowering (S3): This scenario evaluates the effects of riverbed lowering caused by upstream damming and sand mining within the VMD delta on inundation in the study area. The anticipated bathymetry for the main Mekong channel within the VMD in 2038 ( $B_{2038}$ ) as derived from Vasilopoulos et al., (2021) has been employed in the scenarios. This riverbed bathymetry for 2038 was generated by incorporating the riverbed bathymetry from 2018 into the riverbed lowering trend observed from 2008 to 2018, as detailed in Vasilopoulos et al., (2021). This results in the riverbed bathymetry for 2038 being lower than that of 2018, with an average decrease of 2.8 m. The cross-sections, spaced approximately every 3 km along the entire Mekong and Bassac channels, for the 2038 bathymetry were then integrated into the model.

Delta Subsidence (S4\_a, S4\_b): Delta Subsidence (S4\_a, S4\_b): These scenarios evaluate the changes in inundation associated with land subsidence in the projected future. It is important to note that, we only assess the impact of groundwater

extraction-induce land subsidence and does not include other contributing factors such as natural subsidence, tectonic movements, or other human activities (Minderhoud et al., 2017); Zoccarato et al., 2018); (Karlsrud et al., 2020). This focus is due to the fact that land subsidence in the CMP is primarily driven by groundwater extraction (Minderhoud et al., 2017; Karlsrud et al., 2020). The spatial map depicting future land subsidence within the VMD is derived from Minderhoud et al., (2020). This dataset includes land subsidence scenarios labeled B1.5 for the year 2050 (B1.5<sub>2050</sub>) and B2 for the year 2100 (B2<sub>2100</sub>). The B1.5 scenario simulates land subsidence under a moderate increase in groundwater extraction, serving as a pathway between the B1 scenario (moderate increase) and the B2 scenario (extreme increase). Both scenarios follow a non-mitigation pathway, where groundwater extraction continues to increase without any reduction measures, leading to greater land subsidence over time (Minderhoud et al., 2020). In this study, we use the land subsidence scenarios B1.5<sub>2050</sub> and B2<sub>2100</sub>, which are referred to as the S4\_a and S4\_b scenarios, respectively. The S4\_a scenario represents an average land subsidence of 0.38 m ( $\sigma$  = 0.21 m), while the S4\_b scenario reflects 1.12 m ( $\sigma$  = 0.59 m) of subsidence in the CMP.

425

430

435

440

445

450

455

These scenarios evaluated the inundation change associated with land subsidence in the future. The spatial map depicting land subsidence within the VMD in the projected future is derived from Minderhoud et al., (2020). This dataset, encompassing land subsidence scenarios labelled as B1.5 for the year 2050 ( $B1.5_{2050}$ ) and B2 for the year 2100 ( $B2_{2100}$ ) in the study by Minderhoud et al., (2020), is denoted in this study as S4\_a and S4\_b scenarios, respectively. The S4\_a and S4\_B scenarios involve the average land subsidence around 0.38 m ( $\sigma$ =0.21 m) and 1.12 m ( $\sigma$ =0.59 m) in the Ca Mau peninsula, respectively.

Sea-level rise (S5\_a, S5\_b): These scenarios evaluated SLR, an inevitable consequence expected to persist for centuries to millennia due to ongoing deep ocean warming and ice sheet melting. However, human activities, particularly the release of greenhouse gases, have unequivocally contributed to global warming (IPCC, 2023). One of the outcomes of this trend is rising sea levels, extensively explored in various studies (e.g., Kopp et al., 2014; Garner et al., 2018; IPCC, 2023). Since SLR is not just a future prediction but a current phenomenon impacting coastal regions worldwide, it requires attention not only for longterm strategic planning but also for immediate emergency readiness and other short-term considerations (Hall et al., 2019). In this study, consistent with the forecasts outlined in the IPCC Sixth Assessment Report (AR6) (Fox-Kemper et al., 2021) (NASA, 2021)-for the Mekong Delta coastal zone, two scenarios for eustatic SLR were developed. These scenarios involve projections of 0.5 m for the mid-century (2050) (referred to as S5 a) and 1.0 m for the end of this century (2100) (referred to as S5 b), under SSP5-8.5 scenarios with low confidence, in comparison with the sea level in the year 2018, respectively. It is note that these projections do not solely rely on future predictions of sea-level rise, but also consider the dynamic processes involved. For instance, the SLR projections derived from the NASA SLR projection tool already account for Vertical Land Motion, including land subsidence, which could impact the regional SLR rates. To avoid potential double-counting, we have ensured that land subsidence is treated as a separate factor in our analysis, accounting for localized variations based on independent datasets. These adjustments are crucial for accurately representing the local context and ensuring that the impacts of subsidence are not inadvertently overestimated. Following this, the values representing sea-level rise scenarios are incorporated into the time series of tidal levels from the year 2018, functioning as downstream boundaries for the model scenarios.

# 2.4.2 Multiple/combined drivers

460 We then ran 2 other scenarios in which we combined drivers, as described below.

**Projected until Mid-Century (S6):** This scenario combined inundation changes when the high upstream flow (observed water flux of 2018) with storm of 1% AEP entering the Bassac River mouth, incorporating lowered riverbed (2038 riverbed bathymetry), subsidence scenario until 2050 and SLR until 2050.

Projected until End of the Century (S7): This scenario combined inundation changes when the high upstream flow (observed water flux of 2018) with storm of 1% AEP entering the Bassac River mouth. This scenario incorporates the lowered riverbed (2038 bathymetry), the severe subsidence scenario until the end of the century (B2\_2100 scenario), and SLR until 2100.

Table 4. Scenarios utilized to explore the impact of elevated upstream water flow, storm surge, anthropogenic riverbed lowering, delta subsidence, and sea-level rise on the risk of inundation for the <a href="#">Ca Mau peninsula CMP</a>.

<u>Scenarios</u>	<u>Upstream discharge</u>	Storm surge	Riverbed lowering	<b>Delta land subsidence</b>	Sea level rise							
S0 (baseline)	$Q_M$	_	_	_	_							
Scenarios base	Scenarios based on individual drivers											
<u>S1</u>	$Q_{20\%}$	_	-	-	_							
<u>S2</u>	$Q_M$	$TC_{1\%\ AEP}$	_	_	_							
S3	$Q_M$	_	$B_{2038}$	_	_							
<u>S4_a</u>	$Q_M$	_	_	B1.5 <sub>2050</sub> _	_							
<u>S4 b</u>	$Q_M$	_	_	B2 <sub>2100</sub>	_							
<u>S5_a</u>	$Q_M$	_	_	_	<u>+ 0.5 m</u>							
<u>S5_b</u>	$Q_M$	_	_	_	<u>+ 1.0 m</u>							
Scenarios based on multiple drivers												
<u>S6</u>	$Q_{20\%}$	$TC_{1\% AEP}$	$B_{2038}$	B1.5 <sub>2050</sub>	<u>+ 0.5 m</u>							
<u>S7</u>	$Q_{20\%}$	$TC_{1\%\;AEP}$	$B_{2038}$	B2 <sub>2100</sub>	<u>+ 1.0 m</u>							

Scenarios	<del>Upstream</del> <del>discharge</del>	Storm surge	Riverbed lowering	Delta land subsidence	Sea level rise
<del>S0 (baseline)</del>	$Q_M$				

Scenarios based on individual drivers									
<del>S1</del>	<del>Q20%</del>								
<u>\$2</u>	$Q_M$	$TC_{1\% AEP}$							
<del>\$3</del>	Q <sub>M</sub>		<i>B</i> <sub>2038</sub>						
<del>S4_a</del>	$Q_M$			<i>B</i> 1.5 <sub>2050</sub>					
S4_b	Q <sub>M</sub>			B2 <sub>2100</sub>					
<del>S5_a</del>	$Q_M$				+ 0.5 m				
S5_b	$Q_M$				+ 1.0 m				
Scenarios based on individual drivers									
<del>S6</del>	$Q_M$	$TC_{1\% AEP}$	<u>₽<sub>2038</sub></u>	<i>₿</i> 1.5 <sub>2050</sub>	<del>0.5 m</del>				
<del>\$7</del>	Q <sub>M</sub>	TC <sub>1% AEP</sub>	<u>₿<sub>2038</sub></u>	B2 <sub>2100</sub>	<del>1.0 m</del>				

# **2.5 Inundation mapping and statistics**

The direct outcome of the 1D flood model <u>scenariossimulations</u> includes include hourly water levels at all computational nodes (~30,000) within the VMD, for a simulation period 1<sup>st</sup> June to 30<sup>th</sup> November for each year <u>simulated</u>. Subsequently, we extracted the maximum water level and utilized it for spatial interpolation in ArcGIS (using the Natural Neighbour method) to create a water level map with a resolution of 5 m across the study area. The maximum inundation map was then derived by subtracting the ground elevation from the DEM of <u>the</u> region. Areas with a depth < 0.1 m are classified as unflooded. These post processing steps were automated using ArcGIS. Flood maps illustrating the change in inundation levels between simulation scenarios (see Section 2.4) have also been derived. Based on this mapping, we estimated flooding area statistics, providing flooding areas corresponding to each of the following 10 classes: below 0.1 m, 0.1 m – 0.4 m, 0.4 m – 0.7 m, 0.7 m – 1.0 m, 1.0 – 1.3 m, 1.3 m – 1.6 m, 1.6 m – 1.9 m, 1.9 m – 2.2 m, 2.2 – 2.5 m, above 2.5 m. Additionally, maps illustrating the increasing risk of flooding by comparing different scenarios with the S0 scenario have been created. We estimated increasing flooding area statistics for the 10 inundation classes: below -0.1 m (reduce the inundation), -0.1 m – 0.1 m

(unchanged), 0.1 m - 0.4 m, 0.4 m - 0.7 m, 0.7 m - 1.0 m, 1.0 - 1.3 m, 1.3 m - 1.6 m, 1.6 m - 1.9 m, 1.9 m - 2.2 m, above 2.2 m.

#### 3 Results

490

495

500

505

510

Spatial maps depicting the maximum water level, inundation, and the inundation change, relative to the baseline, are shown in Fig. 54, 6-5 and 76, respectively, for each scenario in the Ca Mau Peninsula Ca Mau Peninsula (CMP). The key results for each of the scenarios are described below. The areas flooded in the Ca Mau Peninsula CMP region under the scenarios are listed in Table 5. The accumulated increase in flooded area, compared to the baseline (S0), is given in Table 6.

In the baseline scenarios (S0), the average maximum water level in the study area could reach 0.81 m ( $\sigma$  =0.44 m), and the peak of the maximum water level could reach 1.8 m in the East Sea coastal zone (Fig. 54). This scenario could result in an average inundation depth of 0.04 m ( $\sigma$  =0.43 m) (Fig. 65). Furthermore, within these baseline scenarios, the estimated flood coverage is about 23.9% of the study area, featuring inundation depths between 0.1 m and 0.4 m (Table 5).

In scenario S1 (which evaluates the impact of high upstream water discharge involved the total annual volume exceedance frequency of approximately 20% within the historical data range from 2000 to 2021), the average maximum water level shows a slight increase, reaching 0.92 m ( $\sigma$ =0.45 m), and the peak of maximum water level could reach 1.92 m in the East Sea coastal zone (Fig. 54). This highlights the small rise in water levels in this coastal area resulting from the combination of high-water discharge and sea water level. Moreover, this scenario results in a rise in average inundation depth to 0.15 m ( $\sigma$ =0.43 m) (Fig. 65), affecting around 27.8% of the area with flood depths between 0.1 m to 0.4 m and nearly 16.2% of study area with inundation depths ranging from 0.4 m to 0.7 m (Table 5). The impact of solely high upstream water discharge results in a 43% increase in the study area where inundation depths range from 0.1 m to 0.4 m compared to the corresponding values in scenario S0 (Fig. 7-6 and Table 6).

In scenario S2 (which evaluates the effect of a storm surge with exceedance probability of 1% AEP reaching the Bassac river River mouth; Fig. 2b1b), the results indicate minimal changes in both the maximum water level and the extent of inundation compared to the baseline scenarios S0 (Figures Fig. 54-76, Table 5-6). This implies that the potential impact of a storm surge reaching the main Mekong channel is likely to be minimal in this area. Similarly, in scenario S3, where the effect of riverbed lowering on the main stream Mekong and Bassac channel is assessed, the findings also demonstrate insignificant alterations in both the maximum water level and the extent of inundation when compared to the baseline scenarios S0 (Figures Fig. 34-56, Table 3).

In scenario S4\_a (which investigates the effects of land subsidence up to 2050), results underscore the importance of land subsidence on area inundation. Specifically, the average inundation level shows an increase, rising from 0.04 m ( $\sigma$  =0.43 m) in the S0 scenarios to 0.42 m ( $\sigma$  =0.44 m).), with peak inundation reaching up to 3.93 m in The peak of inundation level could

reach 3.93 m in the vicinity of Ca Mau city (Fig. 65). In this scenarioIn addition, it is projected that the inundated area would cover approximately 30.8% of the study area, with flood depths ranging from 0.1 m to 0.4 m (Table 5). Furthermore, this land subsidence scenarios could increase the flooding risk by an average of 0.38 m ( $\sigma$  =0.21 m), with a maximum increase in flooding risk of 0.94 m compared compared to the baseline S0 scenarios to that in the base scenarios S0 (Fig. 76) and expanding inundation depths by 0.1–0.4 m across 43.3% of the study area compared to the baseline S0 scenarios (Table 6). More specifically, the effects of land subsidence projected until 2050 could lead to an expansion of 43.3% of the study area, experiencing an increase in inundation depths ranging from 0.1 m to 0.4 m compared to the baseline scenarios S0. Additionally, approximately 20.3% and 9.1% of the study area could see rises in inundation depths ranging from 0.4 m to 0.7 m and 0.7 m to 1.0 m, respectively, compared to the baseline scenarios S0 (Table 6).

In scenario S4\_b (which analyses the impact of land subsidence up to the end of this century), the results demonstrate a noticeable increase in inundation both spatially and in magnitude. Specifically, the projected land subsidence  $\frac{1}{2}$  by 2100-could elevate the average inundation depth to 1.15 m ( $\sigma$  =0.67 m) (Fig. 65), affecting 7.9% of the study area with inundation depths between 0.1–0.4 m, while 17.6% and 19.8% would face depths of 0.4–0.7 m and 0.7–1.0 m, respectively. This would encompass an estimated 7.9% of the study area, with inundation depths ranging from 0.1 m to 0.4 m, while approximately 17.6% and 19.8% of the area would experience depths ranging from 0.4 m to 0.7 m, and from 0.7 m to 1.0 m, respectively. Moreover, 1.9% of the study area is expected to encounter inundation depths exceeding 2.5 m (Table 5). Consequently, this land subsidence level could increase the flooding by an average of 1.12 m ( $\sigma$  =0.59 m), with the maximum increase in flooding risk being 2.44 m compared to those in the base scenarios S0 (Fig. 76). Additionally, it could expand the area experiencing 0.4–0.7 m of additional inundation by 22.8%, while 6.4% of the region could face water depths exceeding 2.2 m relative to the baseline S0 (Table 6). The effects of land subsidence up to 2100 may lead to a 22.8 % expansion of the area, where inundation depths increase ranging from 0.4 m to 0.7 m compared to those in the base scenarios S0. Additionally, approximately 6.4% of the study area, could experience inundation depths exceeding 2.2 m in comparison with the base scenarios S0 (Table 6).

In scenario S5\_a (which evaluates the impact of a SLR up to 2050 with a value of 0.5 m), the results indicate that the increase in sea level could elevate the average maximum water level up to 1.32 m ( $\sigma$ =0.45 m), with the maximum water level reaching 2.30 m in the East Sea coastal zone (Fig. 54). Moreover, this rise in sea level also results in an increase in the average inundation depth by 0.55 m ( $\sigma$ =0.43 m) (Fig. 65), affecting approximately 23.9% of the study area with inundation depths ranging from 0.1 m to 0.4 m (Table 5). This scenario exacerbates the risk of inundation at higher levels, impacting around 29.9% of the study area with inundation depths ranging from 0.4 m to 0.7 m and nearly 20.4% of the study area with inundation depths ranging from 0.7 m to 1.0 m (Table 5). Compared to the S0 baseline scenario, a 0.5 m sea level rise could elevate both the average and peak maximum water levels by 0.51 m ( $\sigma$ =0.03 m) and 0.62 m, respectively (Fig. 6). Additionally, this sea level

rise could expand inundation in 86.7% of the study area, with water depths increasing by 0.4–0.7 m relative to the S0 scenario (Table 6).

Regarding the comparison with corresponding values in S0 scenarios, it is highlighted that the sea level rise of 0.5 m could increase both the average and peak of maximum water level to 0.51 m (σ = 0.03 m) and 0.62 m respectively, in comparison with the corresponding values in S0 scenarios (Fig. 7). Furthermore, the influence of a sea level rise of 0.5 m could lead to an expansion in the 86.7% of study area, where the inundation depths increase ranging from 0.4 m to 0.7 m compared to those in the S0 scenarios (Table 6).

550

555

560

565

570

In scenario S5\_b (which examines the impact of a 1.0 m sea level rise by 2100), the findings reveal that the results show that the sea level rise raises both the average maximum water level to 1.83 m ( $\sigma$  = 0.44 m) and the peak maximum water level to 2.80 m. As a result, nearly the entire study area is inundated, with an average inundation depth of 1.06 m ( $\sigma$  = 0.43 m) and a peak depth of 4.45 m. About 28.7% of the area experiences inundation depths ranging from 0.7 m to 1.0 m, while the risk of severe flooding increases, affecting 28.0% of the region with depths ranging from 1.0 m to 1.3 m that this increase in sea level elevates the average maximum water level and peak of maximum water level to 1.83 m ( $\sigma$  = 0.44 m) and 2.80 m respectively. Consequently, almost the entire study area is inundated, with an average inundation depth of 1.06 m ( $\sigma$  = 0.43 m) and a peak maximum inundation depth of 4.45 m. In this scenario, approximately 28.7% of the study area experiences inundation depths ranging from 0.7 m to 1.0 m. However, it exacerbates the risk of inundation at higher levels, affecting around 28.0% of the study area with inundation depths ranging from 1.0 m to 1.3 m (Table 5). Compared to the S0 scenarios, a 1.0 m sea level rise would raise the average and peak maximum water levels by 1.02 m ( $\sigma$  = 0.03 m) and 1.20 m, respectively (Fig. 6). Additionally, this sea level rise would expand inundation across 78.3% of the study area, with water depths increasing from 0.7 m to 1.0 m, while 19.4% of the region would experience depths between 1.0 m and 1.3 m compared to the S0 scenarios (Table 6).

Regarding the increase in inundation compared to the corresponding values in S0 scenarios, it is observed that a sea level rise of 1.0 m could elevate both the average and peak of the maximum water level to 1.02 m ( $\sigma = 0.03 \text{ m}$ ) and 1.20 m, respectively, compared to the corresponding values in S0 scenarios (Fig. 7). Furthermore, the impact of a SLR of 1.0 m could lead to an expansion in the area comprising 78.3% of the study area, where inundation depths increase ranging from 0.7 m to 1.0 m, and 19.4% of the study area, where inundation depths increase ranging from 1.0 m to 1.3 m, compared to those in the S0 scenarios (Table 6).

In <u>combined</u> scenarios S6 (which combine a series of drivers up to 2050; Table 4), the combined factors drive the average maximum water level up to 1.33 m ( $\sigma$  =0.43 m), with the peak of maximum water level reaching 2.31 m in the East Sea coastal zone (Fig. 54). Additionally, these combined factors result in an average inundation depth of 0.91 m ( $\sigma$  =0.44 m), with the maximum inundation depth reaching up to 4.39 m (Fig. 65). Most areas experiencing inundation depths ranging from 0.7 m to 1.0 m cover 30.0% study area, with nearly 0.2% of study area experiencing inundation depths higher than 2.5 m (Table 5). It is noteworthy that the areas experiencing high inundation depths are in the vicinity of Ca Mau city, where the population

density is high, making these regions particularly vulnerable to the impacts of flooding. Regarding the increase in inundation compared to corresponding values in S0 scenarios, it is highlighted that these combined factors could elevate the average and peak of maximum water level to 0.88 m (σ =0.22 m) and 1.38 m respectively, in comparison compared to to the corresponding values in S0 scenarios (Fig. 76). Furthermore, the influence of these combined factors could lead to an expansion in the area of 38.8% of study area where the increasing inundation depths range from 0.7 m to 1.0 m, while there are 3.4% study area where the increasing inundation depths range from 1.3 m to 1.6 m compared to those in the S0 scenarios. (For further details, see Table 6).

In scenarios S7 (which combines a series of drivers up to 2100; Table 4), these combined factors could result in substantial inundation in the Ca Mau peninsula CMP, driving the average maximum water level up to 1.85 m ( $\sigma$  =0.43 m), with the peak of maximum water level reaching up to 2.81 m in the East Sea coastal zone (Fig. 54). This scenario could also result in an average inundation depth of 2.20 m ( $\sigma$  = 0.68 m) (Fig. 5). A substantial portion of the study area (31.3%) could experience inundation depths exceeding 2.5 m (Table 5), with particularly high inundation depths (up to 6.12 m) occurring in the vicinity of Ca Mau city. Additionally, these combined factors could lead to an average inundation depth of 2.20 m ( $\sigma$  =0.68 m) (Fig. 6). Most areas experiencing inundation depths higher than 2.5 m could cover 31.3% of study area (Table 5). It is notable that the areas experiencing high inundation depths reaching up to 6.12 m are in the vicinity of Ca Mau city.

585

Regarding the increase in inundation compared to corresponding values in S0 scenarios, it is highlighted that these combined factors could elevate the average and peak of maximum water level to 2.16 m (σ =0.62 m) and 3.48 m respectively, in comparison to the corresponding values in S0 scenarios (Fig. 76). Furthermore, the influence of these combined factors could lead to an expansion in the area of 2.6% of study area with the increasing inundation depths ranges from 1.0 m to 1.3 m, while there are nearly 40.4% of study area where the increasing inundation depths exceed 2.2 m compared to those in the S0 scenarios.

For further details, please refer to Table 6.

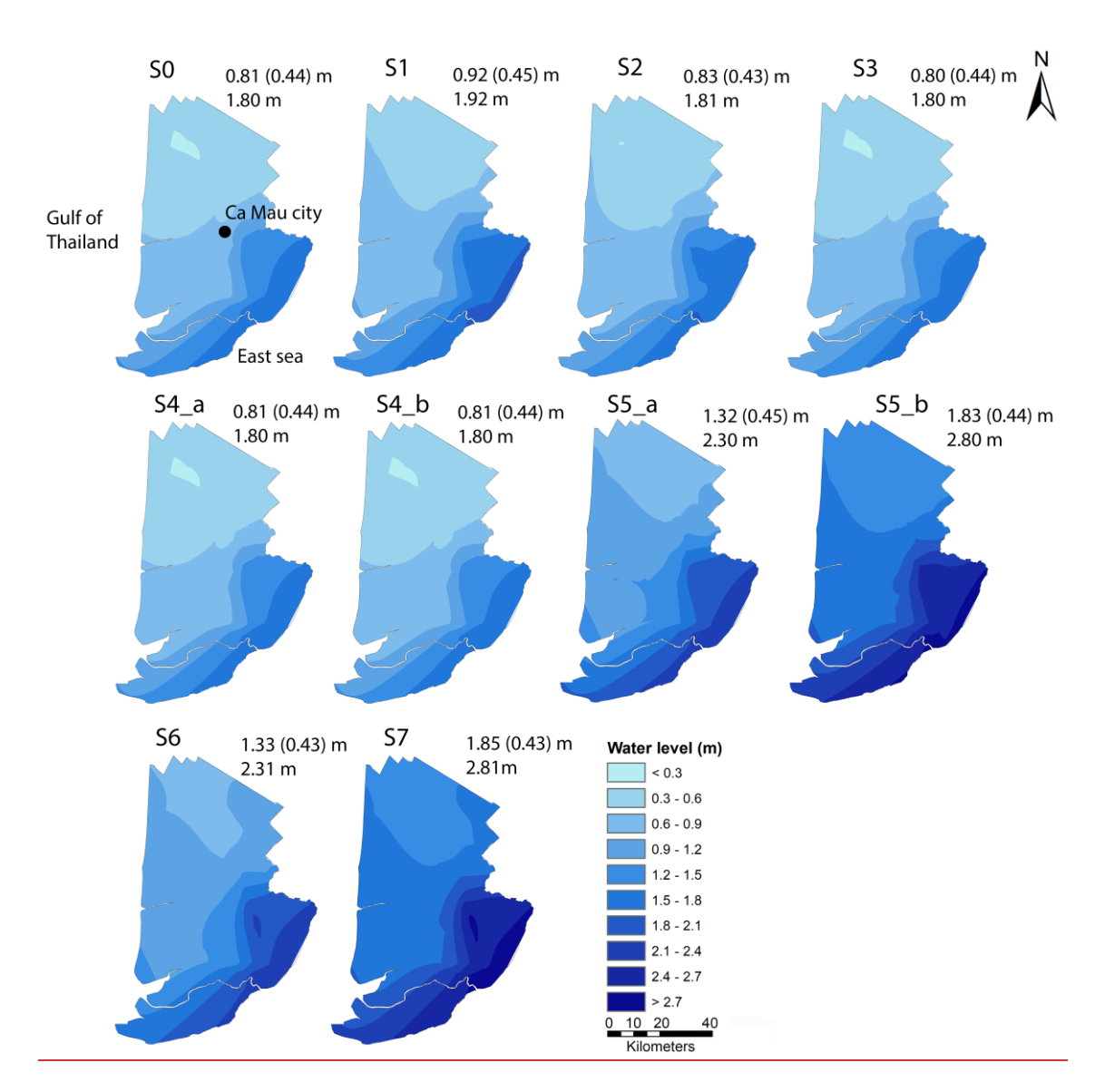


Figure 54. The map depicting the maximum water levels in the Ca Mau Peninsula (Ca Mau Peninsula CMP) under various scenarios. The number in each panel present the average maximum water level (m) and standard deviation (m) (top), along with the peak of these maximum water levels (bottom).

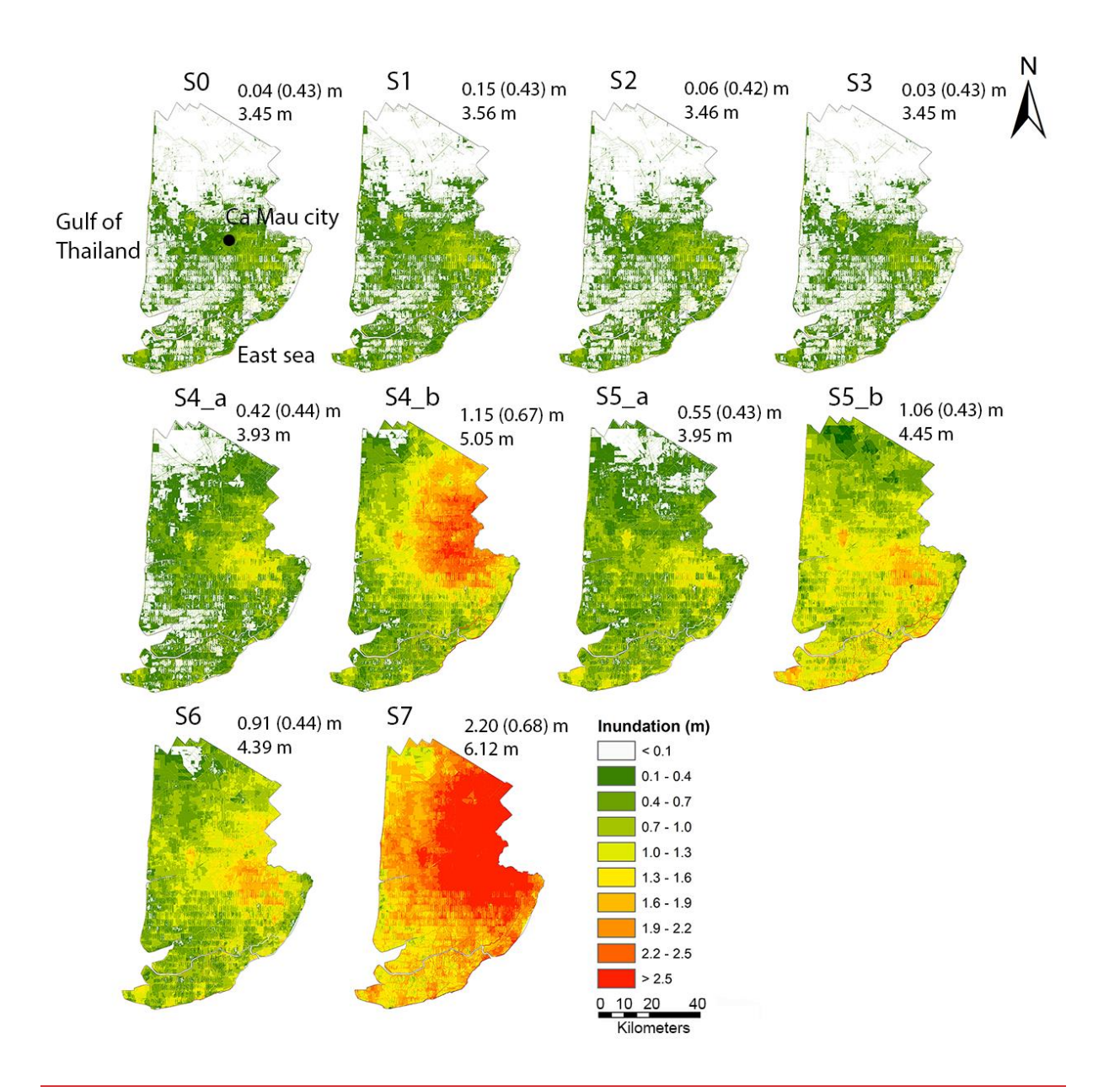


Figure 65. The map illustrating the risk of iMaps of inundation depth in the Ca Mau Peninsula CMP across different scenarios. The number in each panel present the mean inundation (m) and standard deviation (m) (top), along with the peak maximum of these inundation level (bottom).

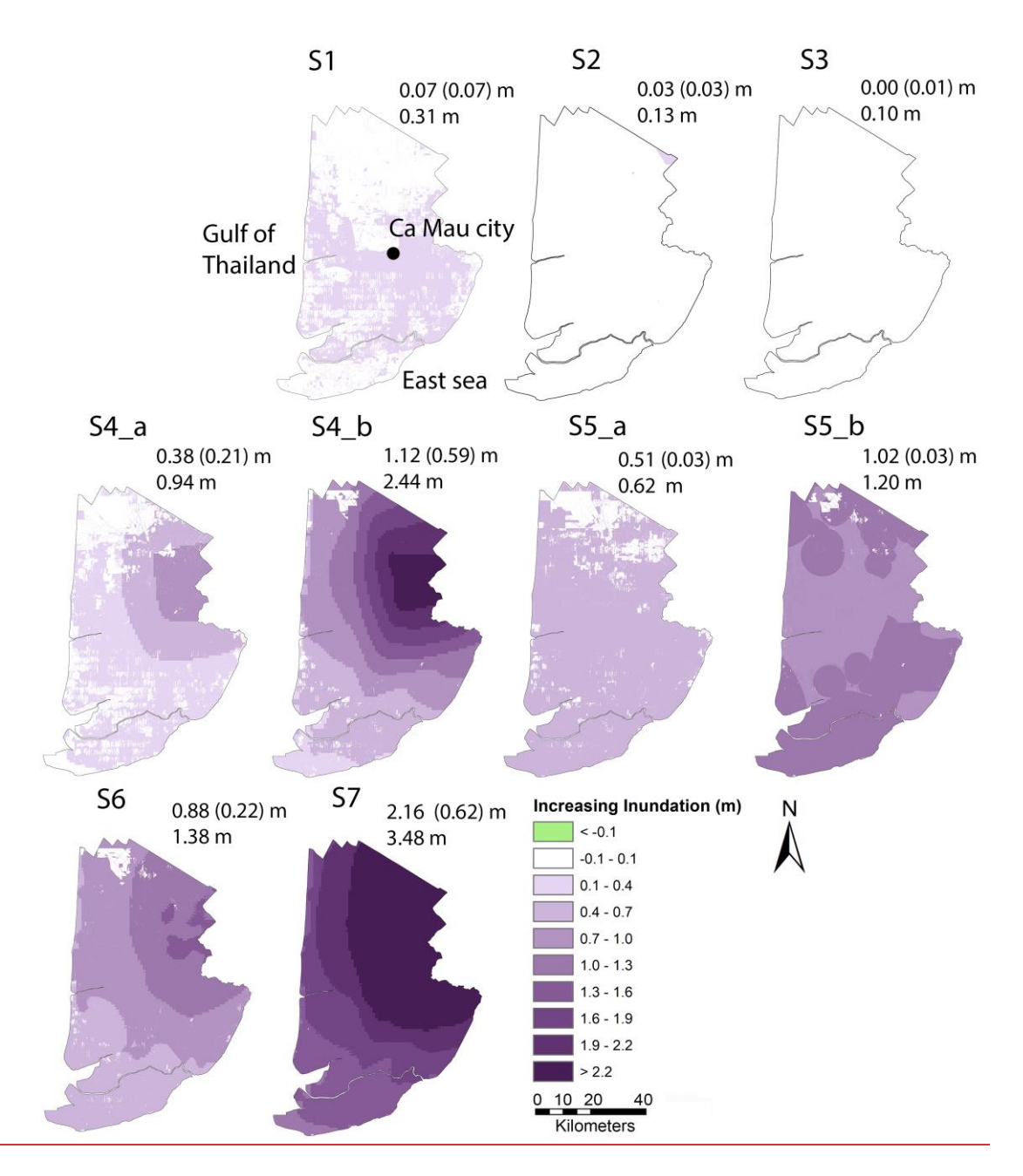


Figure 6. The map illustrating the increasing risk of inundation in the CMP across different scenarios in comparison with the baseline scenarios (S0). The number in each panel present the mean increasing of inundation level (m) and standard deviation (m) (top), along with the peak of these increasing of inundation level (bottom).

# O Table 5. The statistics on the flooded area at different levels in the Ca Mau Peninsula CMP region in our model scenarios

Level (m)		Relative flooded area (%)										
	<u>S0</u>	<u>S1</u>	<u>S2</u>	<u>S3</u>	<u>S4 a</u>	<u>S4 b</u>	<u>S5 a</u>	<u>S5 b</u>	<u>S6</u>	<u>S7</u>		
<u>0.1- 0.4</u>	<u>23.9</u>	<u>27.8</u>	<u>25</u>	<u>23.7</u>	<u>30.8</u>	<u>7.9</u>	<u>23.9</u>	<u>3.2</u>	<u>5.8</u>	0		
0.4- 0.7	<u>11.9</u>	<u>16.2</u>	<u>12.2</u>	<u>11.8</u>	<u>22.8</u>	<u>17.6</u>	<u>29.9</u>	<u>13.3</u>	<u>23.4</u>	<u>0.1</u>		
<u>0.7- 1.0</u>	<u>3.2</u>	<u>5.9</u>	<u>3.8</u>	<u>3.2</u>	<u>12.6</u>	<u>19.8</u>	<u>20.4</u>	<u>28.7</u>	<u>30</u>	<u>1.2</u>		
<u>1.0- 1.3</u>	1	<u>1.7</u>	<u>1.2</u>	1	<u>6</u>	<u>15.3</u>	<u>8.4</u>	<u>28</u>	<u>20.2</u>	<u>5</u>		
<u>1.3- 1.6</u>	0.3	0.6	<u>0.4</u>	0.3	<u>1.7</u>	9.8	<u>2.6</u>	<u>15.8</u>	<u>10.1</u>	<u>13.6</u>		
<u>1.6- 1.9</u>	0.2	0.2	0.2	0.2	<u>0.5</u>	<u>9.9</u>	0.8	<u>6</u>	<u>4.7</u>	<u>19.3</u>		
<u>1.9- 2.2</u>	<u>0.1</u>	0.2	<u>0.1</u>	<u>0.1</u>	<u>0.2</u>	<u>7.4</u>	0.3	<u>1.9</u>	<u>1.4</u>	<u>17.4</u>		
<u>2.2- 2.5</u>	<u>0.1</u>	<u>0.1</u>	<u>0.1</u>	<u>0.1</u>	<u>0.1</u>	<u>6.5</u>	0.2	<u>0.6</u>	0.5	<u>11.2</u>		
<u>&gt;2.5</u>	0	<u>0</u>	<u>0</u>	<u>0</u>	<u>0.1</u>	<u>1.9</u>	<u>0.1</u>	0.3	0.2	<u>31.3</u>		

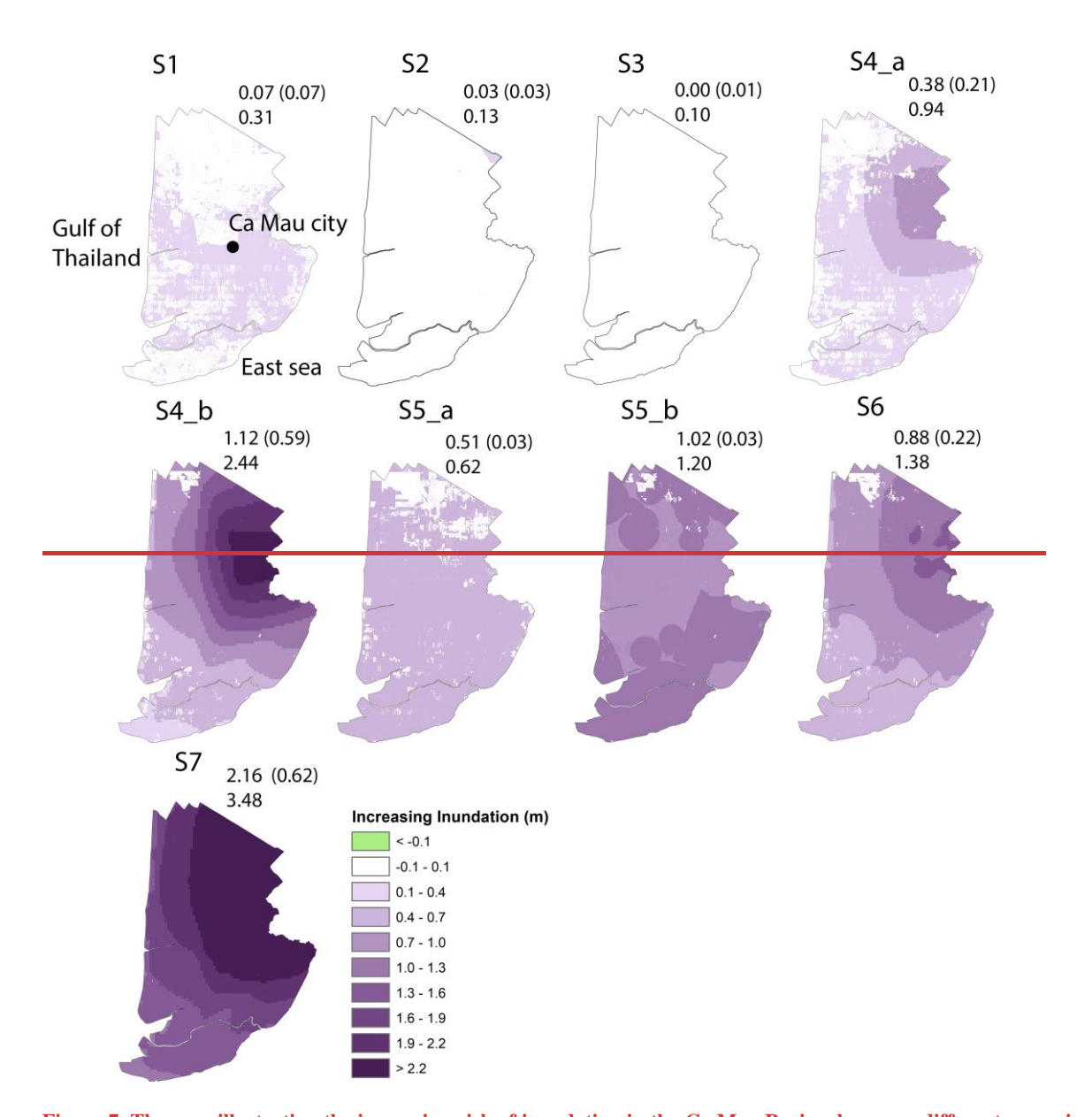


Figure 7. The map illustrating the increasing risk of inundation in the Ca Mau Peninsula across different scenarios in comparison with the baseline scenarios S0. The number in each panel present the mean increasing of inundation level (m) and standard deviation (m) (top), along with the peak of these increasing of inundation level (bottom).

Table 6. The percentage increase in area of flooding in each model scenario, compared to the baseline scenario (S0) at different levels in the Ca Mau Peninsula CMP region

	Accumulated Relative increase in flooded area (%)										
Level (m)	S1	S2	S3	S4_a	S4_b	S5_a	S5_b	S6	S7		
0.1- 0.4	43.0	0.4	0	43.3	5.5	0	0	0	0		
0.4- 0.7	0	0	0	20.3	22.8	86.7	0	28.8	0		
0.7- 1.0	0	0	0	9.1	21.0	0	78.3	38.8	0		
1.0- 1.3	0	0	0	0	13.5	0	19.4	25.3	2.6		
1.3- 1.6	0	0	0	0	9.3	0	0	3.4	20.1		
1.6- 1.9	0	0	0	0	8.7	0	0	0	19.1		
1.9- 2.2	0	0	0	0	8.7	0	0	0	18.9		
>2.2	0	0	0	0	6.4	0	0	0	40.4		

#### 4 Discussion

The aforementioned findingsThe simulation results underscore the potential anthropogenic impact on the evolution of the inundation regime across the Ca Mau Peninsula (Ca Mau peninsula CMP). Specifically, while riverbed lowering in the primary Mekong rivers and storm surges along the mainstream Mekong River are not expected to substantially impact the inundation patterns in this region, the effect of high-water discharge has caused a slight rise in inundation, ranging from 0.1 to 0.3 m. These minimal impacts are largely due to the fact that high-water discharge, riverbed lowering, and storm surges are concentrated in the upstream regions or in the main Mekong and Bassac Rivers. Given the study area's position further from these main rivers and closer to the coastal zone, these impacts tend to diminish. These results suggest that the influences of riverbed lowering in the primary Mekong channel, and the occurrence of storm surges along the mainstream Mekong River are unlikely to significantly affect the inundation regime in this region, while high water discharge did cause the inundation in this study area to rise only by approximately 0.1 0.3 m. The minimal impacts can be attributed to the prominence of high-water discharge, riverbed lowering, and storm surges primarily occurring in the upstream region and in the main Mekong and Bassac channels. Since the study area is situated farther from these channels and closer to the sea on both sides, these impacts tend to diminish. However, the results emphasizes that land subsidence and tidal influence combined with SLR will be the primary factors driving the escalation of the inundation regime in the Ca Mau peninsula CMP in the future, both in extent and

magnitude. In the projected future by the mid-century, under the S6 scenarios, a combination of high-water discharge, storm surge, land subsidence, and sea level rise are projected to inundate 96% of the Camau-PeninsulaCMP, with an average inundation depth of 0.91 m ( $\sigma$  = 0.44 m). Looking towards the end of the  $\frac{21^{st}}{21^{st}}$  century under the S7 scenarios, the compounded effects of high-water discharge, storm surge, land subsidence, and a sea level rise are expected to inundate 99% of the Camau-PeninsulaCMP, with an average inundation depth of 2.20 m ( $\sigma$  = 0.68 m). However, it should be noted that these projections are based on the SSP5-8.5 scenarios, which represent the very worst case with low confidence low likelihood, high impact situations. The ramifications of this increasing trend in inundation are now deliberated in relation to the region's future sustainability and its capacity to adapt to present and future transformationschanges.

The increasing inundation resulting from land subsidence and SLR poses a considerable threat of saltwater intrusion into inland regions, which will have severe consequences for agriculture, aquaculture, and infrastructure within the CMP. This area is not only economically important but also home to one of the most diverse natural ecosystems in the Mekong Delta, with over 79,100 hectares of mangrove forests that play a vital role in maintaining the region's ecological balance. These mangrove forests are essential for protecting coastal zones, regulating freshwater flow, and supporting local biodiversity. However, recent years have seen substantial anthropogenic pressure on this ecosystem, particularly from the development of transportation infrastructure, irrigation systems, and water control structures. These developments have led to considerably degradation of the mangrove forests (Son et al., 2015; Hauser et al., 2020; Thuy et al., 2023), further compounded by the potential rise in inundation levels driven by land subsidence and SLR. This combination of factors threatens to accelerate the loss of these critical ecosystems, undermining their ability to provide natural coastal defence, support biodiversity, and mitigate the effects of climate change (Barbier et al., 2008; Temmerman et al., 2013; Jones et al., 2020; Sunkur et al., 2023).

Although land subsidence and SLR contribute to elevation loss and increased inundation, they may also create conditions favourable for sediment deposition in flooded areas. This sediment trapping mechanism has the potential to partially offset elevation loss over time, thereby influencing future inundation depths. However, the effectiveness of this natural compensatory process is significantly constrained by the sharp reduction in sediment flow from upstream rivers, largely due to damming (Kondolf et al., 2014). These dams have resulted in a projected 57% decrease in suspended sediment flux, from 99 Mt yr<sup>-1</sup> (1980-2009) to 43 Mt yr<sup>-1</sup> by 2020-2029 (Bussi et al., 2021). Sediment transport is crucial for maintaining coastal stability, replenishing eroded areas, and preserving elevation. The decline in sediment supply, driven by upstream dams and other human activities, has worsened the region's vulnerability, accelerating coastal erosion and shoreline retreat (Anthony et al., 2015; (Tu et al., 2019).

In addition, the study also reveals concerns regarding the region's infrastructure, particularly road construction. According to the national North-South Expressway's design specifications for the period 2021-2025 (No: 912/QĐ-BGTVT), the road crest is set 2.2 m above mean sea level in the Ca Mau area (Fig. 1a). However, land subsidence projections of approximately 0.77 m by mid-century and 2.34 m by the end of the century could potentially lower the road crest to 1.43 m and -0.14 m,

respectively. These reductions may not ensure adequate protection, especially considering predicted maximum water levels of approximately 1.59 m by 2050 and 2.20 m by 2100. This assessment is based on Vietnam's road construction standards (TCVN 4054: 2005). Furthermore, the development of infrastructure contributes additional pressure to the deltaic land surface, exacerbating land subsidence in these areas.

685

690

695

700

705

710

715

To mitigate the impacts of flooding caused by SLR and land subsidence in the CMP, it is crucial to implement a combination of sustainable strategies that address both the natural and anthropogenic drivers of flood risk. A primary focus must be on reducing groundwater extraction, the leading cause of land subsidence in the region (Minderhoud et al., 2020). This is critical not only for mitigating land subsidence but also for enhancing the area's resilience to the escalating impacts of climate change (Minderhoud et al., 2020). Additionally, increasing sediment flow from upstream rivers is essential for both replenishing eroded coastal areas and counteracting the effects of land subsidence. By improving sediment management in river systems, such as restoring natural sediment transport pathways and removing barriers like dams, the flow of sediment can be enhanced. Moreover, implementing water-saving technologies, such as efficient irrigation systems and the upgrading of water channels from the Bassac River, can significantly reduce the demand for groundwater in agriculture and domestic use. Developing alternative water sources, such as, rainwater harvesting, desalination, and surface water reservoirs, which can reduce dependency on groundwater, ensuring reliable water supplies during periods of drought or high demand. In parallel, restoring and protecting the natural balance between saltwater and freshwater systems is essential. The creation or rehabilitation of tidal marshes and mangrove forests along the coastline can serve as natural barriers, filtering salinity, protecting against erosion and storm surges, and providing critical habitat for biodiversity while sustaining local livelihoods (Barbier et al., 2008; Temmerman et al., 2013; Jones et al., 2020; Sunkur et al., 2023; Dominicis et al., 2023). In addition, the integration of engineered infrastructure, including tidal barriers, levees, and dikes, can help prevent saltwater intrusion and manage flood risks, particularly in areas most vulnerable to the effects of SLR. Community engagement is also equally important in ensuring the long-term success of these strategies. Raising awareness about the negative impacts of excessive groundwater extraction and the benefits of sustainable water use can foster local participation in conservation efforts. Educational campaigns and training programs can also empower local stakeholders to adopt water-saving practices, contributing to the sustainable management of this vital resource. Finally, investing in robust monitoring systems is essential for tracking groundwater levels, land subsidence rates, and water usage patterns. Accurate, real-time data can inform effective decision-making, enabling authorities to prioritize interventions and manage resources efficiently. By integrating these natural, infrastructural, and community-based strategies, the CMP can build resilience against flooding, safeguard its ecosystems, and ensure the sustainability of its agricultural and aquacultural industries, even in the face of rising seas and land subsidence. The rising inundation resulting from land subsidence and SLR has the potential to cause saltwater intrusion into the inland regions, impacting agriculture, aquaculture, and infrastructure in the Ca Mau peninsula. Moreover, the Ca Mau peninsula remains one of the areas with the richest natural ecosystem in the VMD, boasting over 79.100 hectares of mangrove forests, which contribute to its unique ecological system. In recent years, the development of transportation infrastructure, irrigation systems, and water control structures has been significantly impacting this ecosystem, leading to its decline (Son et al., 2015; Hauser et al. 2020; Thuy et al., 2023). Combined with the potential increase in inundation in these areas, it could further exacerbate the degradation of this ecosystem. Therefore, the effective protective measures are necessary to safeguard this ecological system.

720

725

745

750

Hence, there's a crucial need to guide spatial development towards creating open areas for water retention and establishing freshwater ecological zones within saline environments to promote sustainable groundwater replenishment for agriculture and aquaculture in the future. <u>Furthermore</u>, it's vital to build and upgrade tidal barrier systems, taking into account the escalating inundation factors in the region, to mitigate the impact of future tidal inundation triggered by rising sea levels.

Furthermore, it's vital to build and upgrade tidal barrier systems, taking into account the escalating inundation factors in the region, to mitigate the impact of future tidal inundation triggered by rising sea levels.

- The findings highlight that Ca Mau city's urban zone (Fig. 2), characterized by its dense population, is most susceptible to flooding, underscoring the urgent need for future flood mitigation strategies. These may include measures like minimizing surface water runoff in urban areas and promoting freshwater use for household needs. Proactive management, prevention, and control of flooding induced by SLR are imperative to guarantee the sustainable growth of coastal and riverside socio-economic zones. This effort contributes significantly to ensuring security, defence, and the protection of lives, property, and livelihoods.
- Furthermore, the results highlight the potential inundation risk in this area concerning road construction standards. For example, according to the design specifications of the national North-South Expressway for the period 2021-2025 (No: 912/QD-BGTVT) in the Ca Mau area, the road's crest is set at 2.2 m above mean sea level in Ca Mau city. However, in scenarios involving land subsidence of approximately 0.77 m and 2.34 m in this area by the middle and end of this century, respectively, the potential crest of the road would decrease to 1.43 m and -0.14 m by the middle and end of this century, respectively. These values may not ensure safety, especially considering the predicted maximum water levels in this area, which are approximately 1.59 m in 2050 and 2.20 m in 2100, respectively. This assessment is based on Vietnam's road construction standards (TCVN 4054: 2005).

Moreover, the Ca Mau peninsula remains one of the areas with the richest natural ecosystem in the VMD, boasting over 79,100 hectares of mangrove forests, which contribute to its unique ecological system. In recent years, the development of transportation infrastructure, irrigation systems, and water control structures has been significantly impacting this ecosystem, leading to its decline (Son et al., 2015; Hauser et al. 2020; Thuy et al., 2023). Combined with the potential increase in inundation in these areas, it could further exacerbate the degradation of this ecosystem. Therefore, the effective protective measures are necessary to safeguard this ecological system. In this study, flood riskhazard in the CMP was assessed using 1D modelling, considering both individual and combined flood-inducing factors. Although the results provide useful insights, it is essential to recognize the inherent uncertainties associated with the model scenarios and methodologies used. One limitation

arises from the use of a one-dimensional model, which calculates water levels in the floodplain through spatial interpolation from the water levels in surrounding channels. While this approach may be less accurate compared to a 2D model. However, by integrating a quasi-2D representation of the floodplains, the model improves its capability to simulate hydrodynamic behaviour more accurately, offering a reasonable estimate when compared to 2D modelling. In addition, the 1D model utilized in this study incorporates extensive data on secondary channels within the Vietnam Mekong Delta (VMD), covering 4,235 river branches with a resolution ranging from 1 km to 3 km per channel across CMP, ensuring an accurate representation of the region's complex hydrodynamics and enabling a detailed spatial depiction of water levels.

755

760

765

770

775

780

The model does not account for long-term sediment transport, which could influence changes in the floodplain area, with sedimentation potentially counteracting land subsidence (Hung et al., 2014; Zoccarato et al., 2018). While this limitation is acknowledged, the study partially addresses it by incorporating predicted bathymetric changes in the main Mekong River up to 2038, considering factors such as sediment deficits and sand mining activities (Vasilopoulos et al., 2021). These adjustments are intended to capture certain aspects of sediment dynamics and their potential impact on the delta.

Although the accuracy of topographic DEMs in the VMD remains a topic of ongoing discussion (Minderhoud et al., 2019), this study utilized a Digital Elevation Model (DEM) for the CMP developed by the Ministry of Natural Resources and Environment (MONRE) in 2008 (Tran et al., 2016). This DEM, with a resolution of 5 m × 5 m, is based on the WGS84 coordinate system and the Hon Dau mean sea level datum, and was created using high-quality survey data, topographic maps, and photogrammetric information (Tran et al., 2016). While this methodology aligns with the TOPO DEM by Minderhoud et al., (2019), which is known for its accuracy at a coarser resolution (500 m  $\times$  500 m), the higher resolution of our DEM is better suited for localized analyses of the CMP, providing greater precision in capturing the region's topography and inundation dynamics. The use of a 5x5 m resolution DEM in this study has provided a detailed representation of the topographical variations within the study area. However, this high level of detail also introduces certain artefacts that become apparent in Fig. 5 and 6. These artefacts stem from the granularity of the DEM dataset, which captures subtle variations in elevation between adjacent cells. Such elevation differences are particularly pronounced in the mapping of inundation levels, where thresholds such as <0.1 m (unflooded; white colour, Fig. 5) and 0.1–0.4 m (flooded; green colour, Fig. 5) highlight the varying extents of inundated areas. While this granularity allows for a more precise delineation of inundation zones, it also introduces abrupt transitions in the inundation extent that may not accurately reflect real-world conditions. These artefacts are especially noticeable in flat or low-lying areas, where small discrepancies in elevation can disproportionately affect the modelled inundation extent. Despite these limitations, the 5x5 m DEM provides valuable insights into the spatial distribution of inundation areas at a resolution suitable for regional-scale assessments. The artefacts observed in this study highlight the importance of balancing DEM resolution with the study's scale and objectives to ensure accurate and reliable outcomes. The assumption that areas with a depth of less than 0.1 m are classified as unflooded is typically used to identify negligible inundation. However, in urban areas, even shallow water depths can become hazardous when associated with high flow velocities. Such conditions can lead to risks, such as infrastructure damage, heightened erosion, and potential threats to public safety. Additionally, the use of a DEM from 2008 introduces a temporal discrepancy when combined with sea level rise (SLR) and land subsidence scenarios derived from 2018 data. Between 2008 and 2018, SLR in the coastal region was relatively small, with an estimated increase of less than 5 cm according to MONRE projections (Tran et al., 2016), which had minimal impact on the analysis. However, land subsidence during this period was more pronounced, with a maximum of 15 cm in certain areas (Minderhoud et al., 2017). Although these changes could introduce slight inaccuracies in the DEM's topography, the variations in relative elevation from 2008 to 2018 remain negligible within the scope of this study. Specifically, sea level rise scenarios range from 0.5 m to 1 m, and land subsidence scenarios range from 0.38 m ( $\sigma$  = 0.21 m) to 1.12 m ( $\sigma$  = 0.59 m), reflecting regional variability. Thus, the relative elevation changes from 2008 to 2018 are considered minimal within the scope of our analysis.

Regarding land subsidence scenarios, this study focuses solely on the impact of groundwater extraction, excluding other factors contributing to land subsidence, such as natural subsidence, tectonic movements, or other human activities (Minderhoud et al., 2017; Zoccarato et al., 2018; Karlsrud et al., 2020). This emphasis is based on the fact that groundwater extraction is the primary driver of land subsidence in the CMP (Minderhoud et al., 2017; Karlsrud et al., 2020). However, it is important to acknowledge that reduced sediment input from upstream could exacerbate natural subsidence processes, particularly through natural compaction, as discussed by Zoccarato et al., (2018). Therefore, while this study does not account for these additional subsidence factors, the broader context of sediment deficits should be considered as a contributing factor to the overall land subsidence in the region.

Finally, the inundation scenarios in this study are based on long-term projections that consider the cumulative impacts of land subsidence and sea level rise up to 2100. While these projections are essential for evaluating future risks and guiding long-term planning, they may not fully account for short-term fluctuations or temporary environmental changes, potentially leading to an overestimation of short-term impacts. Although the focus on long-term trends offers valuable insights into future scenarios, further research that includes short-term variability is needed to provide a more comprehensive understanding of the region's vulnerability to flooding and land subsidence in the near term.

#### 55 Conclusions

785

790

795

800

805

810

The <u>Ca Mau peninsula (Ca Mau peninsula CMP)</u> is identified as one of the most promising economic hubs for agriculture and aquaculture within both the <u>Vietnamese</u> Mekong Delta (VMD) region and Vietnam as a whole. Nonetheless, <u>this area also experiences considerable flood risk these areas also face considerable vulnerability to flooding</u>. <u>This study aimed to predict</u>

inundation patterns across the CMP by modelling the impacts of various flood-inducing factors, both individually and in combination. This study focused on predicting the inundation patterns across the Ca Mau peninsula under different drivers using a modelling approach. The 1D hydrodynamic model, initially proposed by Dung, (2011) Dung et al., (2011), has been enhanced with updated with bathymetry data of the main Mekong River bed within the VMD in 2018, and with infrastructure features (such as dykes, sluices) in 2019 across the entire VMD. The model has been fully calibrated and validated to accurately simulate the flood regime within the VMD and study area.

The findings indicate that factors such as increased high-water flow from upstream, riverbed lowering in the main Mekong channel, and occurrences of storm surges along the mainstream Mekong River are unlikely to substantial impact the inundation dynamics in this CMP. The findings indicate that factors such as increased high water flow from upstream, alterations in the riverbed of the main Mekong channel, and occurrences of storm surges along the mainstream Mekong River are unlikely to significantly impact the inundation dynamics in this southern region of the VMD. However, the study underscores that land subsidence, rising sea levels, and their combined effects are primary drivers behind the escalation of inundation events in the Ca Mau peninsula CMP, both in terms of extent and intensity, in the foreseeable future.

A projected SLR of 0.5 m by the year 2050 is anticipated to result in an 87% inundation of the study area, with an average depth of 0.55 m ( $\sigma$  =0.43 m). Looking ahead to the end of the century, where the estimated SLR could reach around 1 m, it is forecasted that 98% of the study area will experience inundation, with an average depth of 1.83 m ( $\sigma$  =0.44 m). Furthermore, iIn the projected future by the mid-century, a compounded effect of factors including high-water discharge (with a total annual volume exceedance frequency of approximately 20%), storm surge (with an annual exceedance probability of 1% AEP along the Bassac river mouth), land subsidence (averaging around 0.38 m ( $\sigma$  =0.21 m), and a SLR of 0.5 m is expected to result in the inundation of 96% of the Camau peninsulaCMP area, with an average inundation depth of 0.91 m ( $\sigma$  =0.44 m). Looking further into the end of the century, under a compounded influence of high-water discharge (with a total volume exceedance frequency of approximately 20%), storm surge (with an annual exceedance probability of 1% AEP along the Bassac river mouth), land subsidence (averaging around 1.12 m ( $\sigma$  =0.59 m)), and a SLR of 1 m, the projected inundation of the Camau peninsulaCMP is expected to encompass 99% of the area, with an average inundation depth of 2.20 m ( $\sigma$  =0.68 m).

These results show that the future potential risks associated with the rising inundation levels in this study area need to be carefully considered concerning the future sustainability of the region and its ability to adapt to both current and forthcoming pressures due to human activity and climate change. This objective of these findings is to provide insight for strategic planners as they contemplate various avenues for spatial development within the <a href="mailto:Ca Mau peninsulaCMP">Ca Mau peninsulaCMP</a>. They represent a crucial foundation for shaping policies and devising investment strategies related to infrastructure systems, including flood defences, tidal defence dykes, and irrigation and especially for safe transportation.—Furthermore, the projected rise in inundation levels in this region, largely attributed to SLR and land subsidence, poses a significant challenge to the preservation of one of the pristine mangrove forest ecosystems in the VMD. This ecosystem is already under threat from ongoing infrastructure

developments in the area. Therefore, it is imperative to implement measurement, planning, and adaptation strategies to address this issue effectively in the future.

# 6 Appendix A

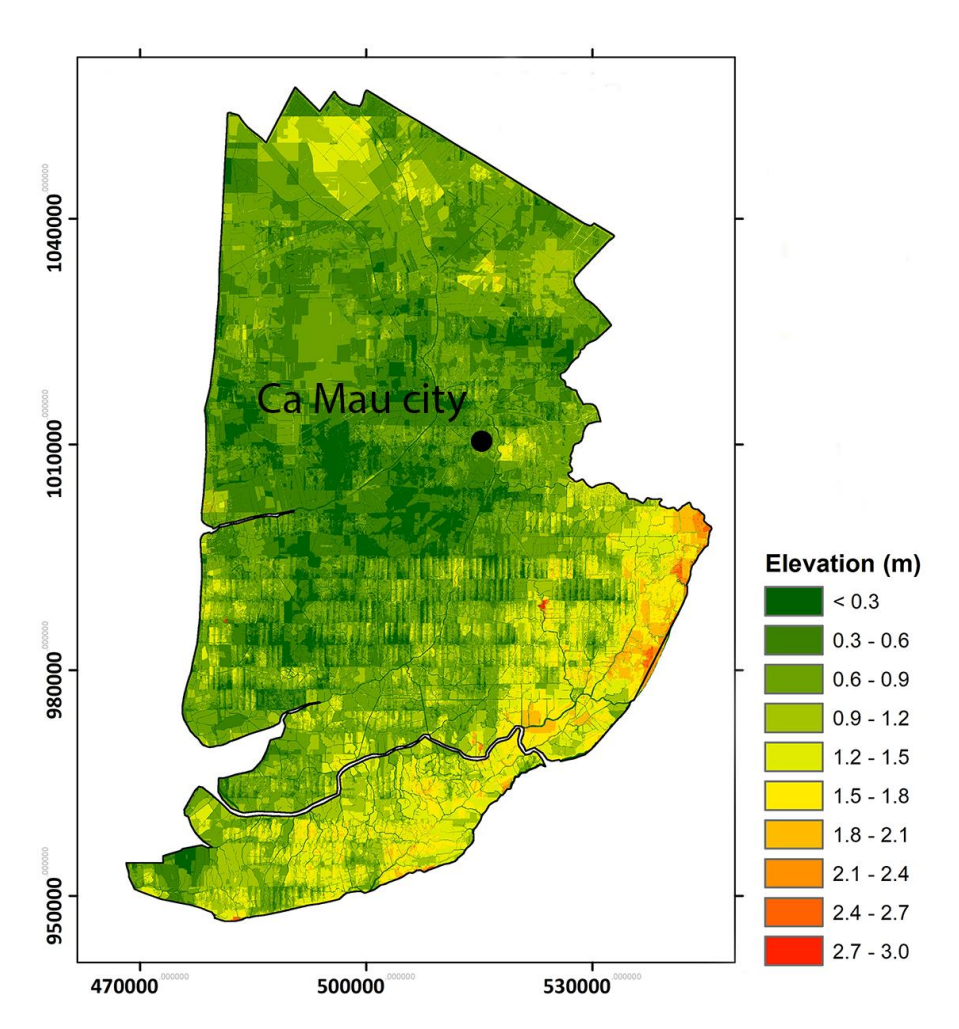


Figure A1. DEM illustrates the flat terrain of the Ca Mau peninsula CMP acquired from the Ministry of Natural Resources and Environment (MONRE) in 2008 (Tran et al., 2016).

Author contribution. Hung Nguyen Nghia: Conceptualization, Methodology, Resources, Visualization, Modelling-work, Formal Analysis, Writing - original draft, Writing - review & editing. Quan Quan Le: Conceptualization, Methodology, Data curation, Modelling-work, Validation, Formal Analysis, Visualization, Writing - review & editing. Dung Viet Nguyen: Conceptualization, Methodology, Investigation, Writing - review & editing. Do Dac Hai: Methodology, Writing - review & editing. Hung Duc Pham: Writing - review & editing. Hong Tan Cao: Writing - review & editing. Toan Quang To: Writing - review & editing. Do Dac Hai: Methodology, Writing - review & editing. Melissa Wood: Conceptualization, Methodology, Writing - review & editing.

Competing interests. The authors declare that they have no conflict of interest

875

Acknowledgments. This study was co-funded by the UK National Environment Research Council (NERC) and the Viet Nam

National Foundation for Science and Technology Development (NAFOSTED) under the grant number: NE/S003150/1. O.Q.L.

was financially supported by the Geography and Environment Department at Loughborough University, UK.

The authors sincerely thank Dr. Philip S.J. Minderhoud for providing land subsidence scenarios for the Mekong Delta. They also extend their gratitude to Dr. Grigorios Vasilopoulos for his assistance in supplying bathymetric data of the Mekong River channels.

870 The authors thanks to Dr. Philip S.J. Minderhoud for his help in providing the land subsidence scenarios in the Mekong Delta.

# References

885

- Anthony, E.J., G. Brunier, M. Besset, M. Goichot, P. Dussouillez, and V. L Nguyen. 2015. "Linking Rapid Erosion of the Mekong River Delta to Human Activities." *Scientific Reports* 5. doi:10.1038/srep14745.
  - Attaher, S. M., M. A. Medany, and A. F. Abou-Hadid. 2009. "Possible Adaptation Measures of Agriculture Sector in the Nile Delta to Climate Change Impacts." *Advances in Science and Research* 3(1): 123–26. doi:10.5194/asr-3-123-2009.
  - Barbier, Edward B., Evamaria W. Koch, Brian R. Silliman, Sally D. Hacker, Eric Wolanski, Jurgenne Primavera, Elise F. Granek, et al. 2008. "Coastal Ecosystem-Based Management with Nonlinear Ecological Functions and Values." *Science* 319(5861): 321–23. doi:10.1126/science.1150349.
    - Best, J. 2019. "Anthropogenic Stresses on the World's Big Rivers." *Nature Geoscience* 12: 7–21. doi:10.1038/s41561-018-0262-x.
- Bevacqua, E., D. Maraun, M. I. Vousdoukas, E. Voukouvalas, M. Vrac, L. Mentaschi, and M. Widmann. 2019. "Higher Probability of Compound Flooding from Precipitation and Storm Surge in Europe under Anthropogenic Climate Change." *Science Advances* 5(9): 1–8. doi:10.1126/sciadv.aaw5531.
  - Bravard, J.P., M. Goichot, and S. Gaillot. 2013. "Geography of Sand and Gravel Mining in the Lower Mekong River." *EchoGéo*: 0–20. doi:10.4000/echogeo.13659.
- Bussi, G., S.E. Darby, P.G. Whitehead, L. Jin, S.J. Dadson, H.E. Voepel, G. Vasilopoulos, et al. 2021. "Impact of Dams and Climate Change on Suspended Sediment Flux to the Mekong Delta." *Science of the Total Environment* 755. doi:10.1016/j.scitotenv.2020.142468.
  - Chen, W.B., and W.C. Liu. 2014. "Modeling Flood Inundation Induced by River Flow and Storm Surges over a River Basin." *Water* 6: 3182–99. doi:10.3390/w6103182.
  - Dang, An T. N., Michael Reid, and Lalit Kumar. 2023. "Coastal Melaleuca Wetlands under Future Climate and Sea-Level Rise Scenarios in the Mekong Delta, Vietnam: Vulnerability and Conservation." *Regional Environmental Change* 23(1). doi:10.1007/s10113-022-02009-8.
  - De Dominicis, Michela, Judith Wolf, Rosanna van Hespen, Peng Zheng, and Zhan Hu. 2023. "Mangrove Forests Can Be an Effective Coastal Defence in the Pearl River Delta, China." *Communications Earth and Environment* 4(1). doi:10.1038/s43247-022-00672-7.
- Dung, N V. 2011. "Multi-Objective Automatic Calibration of Hydrodynamic Models Development of the Concept and an Application in the Mekong Delta." *PhD Thesis* (978-3-942036-11–5): 133. http://elib.uni-stuttgart.de/opus/volltexte/2012/6831/.

- Edmonds, D. A., R. L. Caldwell, E. S. Brondizio, and S.M.O. Siani. 2020. "Coastal Flooding Will Disproportionately Impact People on River Deltas." *Nature Communications* 11: 1–8. doi:10.1038/s41467-020-18531-4.
- Erban, L.E., S.M. Gorelick, and H.A. Zebker. 2014. "Groundwater Extraction, Land Subsidence, and Sea-Level Rise in the Mekong Delta, Vietnam." *Environmental Research Letters* 9. doi:10.1088/1748-9326/9/8/084010.
  - Eslami, S., P. Hoekstra, N.N. Trung, S.A. Kantoush, D.V. Binh, D.D. Dung, T.T. Quang, and M.V.D Vegt. 2019. "Tidal Amplification and Salt Intrusion in the Mekong Delta Driven by Anthropogenic Sediment Starvation." *Scientific Reports* 9: 1–10. doi:10.1038/s41598-019-55018-9.
- Fox-Kemper, B., Hewitt, H. T., Xiao, C., Aðalgeirsdóttir, G., Dri- jfhout, S. S., Edwards, T. L., Golledge, N. R., Hemer, M., Kopp, R. E., Krinner, G., Mix, A., Notz, D., Nowicki, S., Nurhati, I. S., Ruiz, L., Sallée, J.-B., Slangen, A. B. A., and Yu, Y. 2021. "Ocean, Cryosphere and Sea Level Change, in: Climate Change 2021: The Physical Science Basis, Contribution of Working Group I to the Sixth Assessment Report of the Intergovernmental Panel on Climate Change, Edited by: Masson-Delmotte, V., Zhai, P., Pirani,." *Cambridge University Press, Cambridge, UK and New York, NY, USA*: 1211–1362. doi:https://doi.org/10.1017/9781009157896.011.
- 920 Ganguli, Poulomi, and Bruno Merz. 2019. "Trends in Compound Flooding in Northwestern Europe During 1901–2014." Geophysical Research Letters 46(19): 10810–20. doi:10.1029/2019GL084220.
  - Garner, Andra J, Jeremy L Weiss, Adam Parris, Robert E Kopp, Jonathan T Overpeck, and Benjamin P Horton. 2018. "Evolution of 21st Century Sea Level Rise Projections." *Earth's Future* (6): 1603–15. doi:10.1029/2018EF000991.
  - "General Statistics Office of Vietnam." 2020. https://www.gso.gov.vn/en/homepage/.

- 925 Giosan, L., J. Syvitski, S. Constantinescu, and J.W. Day. 2014. "Climate Change: Protect the World's Deltas." *Nature* 516: 31–33. doi:10.1038/516031a.
  - Gugliotta, M., Y. Saito, V.L. Nguyen, T.K.O. Ta, R. Nakashima, T. Tamura, K. Uehara, K. Katsuki, and S. Yamamoto. 2017. "Process Regime, Salinity, Morphological, and Sedimentary Trends along the Fluvial to Marine Transition Zone of the Mixed-Energy Mekong River Delta, Vietnam." *Continental Shelf Research* 147: 7–26. doi:10.1016/j.csr.2017.03.001.
- Hackney, C.R., G. Vasilopoulos, S. Heng, V. Darbari, S. Walker, and D.R. Parsons. 2021. "Sand Mining Far Outpaces Natural Supply in a Large Alluvial River." *Earth Surface Dynamics* (May): 1–20. doi:https://doi.org/10.5194/esurf-2021-39.
  - Haigh, Ivan D., E. M.S. Wijeratne, Leigh R. MacPherson, Charitha B. Pattiaratchi, Matthew S. Mason, Ryan P. Crompton, and Steve George. 2014. "Estimating Present Day Extreme Water Level Exceedance Probabilities around the Coastline of Australia: Tides, Extra-Tropical Storm Surges and Mean Sea Level." *Climate Dynamics* 42(1–2): 121–38. doi:10.1007/s00382-012-1652-1.
  - Hall, J. A., C.P. Weaver, J. Obeysekera, M. Crowell, R.M. Horton, R.E. Kopp, J. Marburger, et al. 2019. "Rising Sea Levels:

- Helping Decision-Makers Confront the Inevitable." *Coastal Management* 47: 127–50. doi:10.1080/08920753.2019.1551012.
- Hauser, Leon T., Leon T Hauser, Nguyen An Binh, Pham Viet Hoa, Nguyen Hong Quan, and Joris Timmermans. 2020. "Gap-940 Free Monitoring of Annual Mangrove Forest Dynamics in Ca Mau Province, Vietnamese Mekong Delta, Using the Landsat-7-8 Archives and Post-Classification Temporal Optimization." *MDPI*. doi:doi:10.3390/rs12223729.
  - Hoang, L.P., H. Lauri, M. Kummu, J. Koponen, M.T.H.V. Vliet, I. Supit, R. Leemans, P. Kabat, and F. Ludwig. 2016. "Mekong River Flow and Hydrological Extremes under Climate Change." *Hydrology and Earth System Sciences* 20: 3027–41. doi:10.5194/hess-20-3027-2016.
- 945 Hung, N.N., J.M. Delgado, A. Güntner, B. Merz, A. Bárdossy, and H. Apel. 2014. "Sedimentation in the Fl Oodplains of the Mekong Delta, Vietnam. Part I: Suspended Sediment Dynamics." 3144: 3132–44. doi:10.1002/hyp.9856.

- IPCC. 2007. "Climate Change 2007: Impacts, Adaptation and Vulnerability. Contribution of Working Group II to the Fourth Assessment Report of the Intergovernmental Panel on Climate Change." M.L. Parry, O.F. Canziani, J.P. Palutikof, P.J. van der Linden and C.E. Hanson, Eds., Cambridge University Press, Cambridge, UK, 976pp. Editorial (Cambridge University Press, Cambridge, UK, 976pp).
- IPCC. 2023. "Climate Change 2023 Synthesis Report, Summary for Policymakers." Contribution of Working Groups I, II and III to the Sixth Assessment Report of the Intergovernmental Panel on Climate Change [Core Writing Team, H. Lee and J. Romero (eds.)], IPCC, Geneva, Switzerland, pp. 1-34,. doi:10.59327/IPCC/AR6-9789291691647.001.
- Jones, Holly P., Barry Nickel, Tanja Srebotnjak, Will Turner, Mariano Gonzalez-Roglich, Erika Zavaleta, and David G. Hole.

  2020. "Global Hotspots for Coastal Ecosystem-Based Adaptation." *PLoS ONE* 15(5): 1–17. doi:10.1371/journal.pone.0233005.
  - Karlsrud, Kjell, Lloyd Tunbridge, Nguyen Quoc Khanh, and Nguyen Quoc Dinh. 2020. "Preliminary Results of Land Subsidence Monitoring in the Ca Mau Province." *Proceedings of the International Association of Hydrological Sciences* 382: 111–15. doi:10.5194/piahs-382-111-2020.
- 960 Kingston, D. G., J. R. Thompson, and G. Kite. 2011. "Uncertainty in Climate Change Projections of Discharge for the Mekong River Basin." *Hydrology and Earth System Sciences* 15: 1459–71. doi:10.5194/hess-15-1459-2011.
  - Kondolf, G. M., Z. K. Rubin, and J. T. Minear. 2014. "Dams on the Mekong: Cumulative Sediment Starvation." *Water Resources Research* 50: 5158–69. doi:10.1002/2013WR014651.
- Kopp, Robert E, Radley M Horton, Christopher M Little, Jerry X Mitrovica, Michael Oppenheimer, D J Rasmussen, Benjamin

  H Strauss, and Claudia Tebaldi. 2014. "Probabilistic 21st and 22nd Century Sea-Level Projections at a Global Network

  of Tide-Gauge Sites." *Earth's Future*: 383–407. doi:doi:10.1002/2014EF000239.

- Kummu, M., X. X. Lu, J. J. Wang, and O. Varis. 2010. "Basin-Wide Sediment Trapping Efficiency of Emerging Reservoirs along the Mekong." *Geomorphology* 119(3–4): 181–97. doi:10.1016/j.geomorph.2010.03.018.
- Lauri, H., H. De Moel, P. J. Ward, T. A. Räsänen, M. Keskinen, and M. Kummu. 2012. "Future Changes in Mekong River Hydrology: Impact of Climate Change and Reservoir Operation on Discharge." *Hydrology and Earth System Sciences* 16: 4603–19. doi:10.5194/hess-16-4603-2012.
  - Leonard, Michael, Seth Westra, Aloke Phatak, Martin Lambert, Bart van den Hurk, Kathleen Mcinnes, James Risbey, et al. 2014. "A Compound Event Framework for Understanding Extreme Impacts." Wiley Interdisciplinary Reviews: Climate Change 5(1): 113–28. doi:10.1002/wcc.252.
- 275 Lu, X.X., M. Kummu, and C. Oeurng. 2014. "Reappraisal of Sediment Dynamics in the Lower Mekong River, Cambodia." Earth Surface Processes and Landforms 39: 1855–65. doi:10.1002/esp.3573.
  - Manh, N. V., N. V. Dung, N. N. Hung, B. Merz, and H. Apel. 2014. "Large-Scale Suspended Sediment Transport and Sediment Deposition in the Mekong Delta." *Hydrology and Earth System Sciences* 18(8): 3033–53. doi:10.5194/hess-18-3033-2014.
- 980 Minderhoud, P. S.J., L. Coumou, G. Erkens, H. Middelkoop, and E. Stouthamer. 2019. "Mekong Delta Much Lower than Previously Assumed in Sea-Level Rise Impact Assessments." *Nature Communications*: 1–13. doi:10.1038/s41467-019-11602-1.
  - Minderhoud, P. S.J., G. Erkens, V. H. Pham, V. T. Bui, L. Erban, H. Kooi, and E. Stouthamer. 2017. "Impacts of 25 Years of Groundwater Extraction on Subsidence in the Mekong Delta, Vietnam." *Environmental Research Letters* 12. doi:10.1088/1748-9326/aa7146.
    - Minderhoud, P.S.J., H. Middelkoop, G. Erkens, and E. Stouthamer. 2020. "Groundwater Extraction May Drown Mega-Delta: Projections of Extraction-Induced Subsidence and Elevation of the Mekong Delta for the 21st Century." *Environmental Research Letters*. doi:https://doi.org/10.1088/2515-7620/ab5e21.
- Moriasi, D. N., J. G. Arnold, M. W. V. Liew, R. L. Bingner, R. D. Harmel, and T. L. Veith. 2007. "Model Evaluation Guidelines for Systematic Quantification of Accuracy in Watershed Simulations." *American Society of Agricultural and Biological Engineers* 50: 885–900.
  - MRC. 2005. "Overview of the Hydrology of the Mekong Basin." (November).

- MRC. 2011. "Flood Situation Report 2011." (36). http://www.mrcmekong.org/assets/Publications/technical/Tech-No36-Flood-Situation-Report2011.pdf (last access: 15/04/2014).
- 995 Nash, J. E., and J. V. Sutcliffe. 1970. "River Flow Forecasting through Conceptual Models Part I A Discussion of Principles." *Journal of Hydrology* 10: pp: 282-290.

- Olbert, Agnieszka I., Joanne Comer, Stephen Nash, and Michael Hartnett. 2017. "High-Resolution Multi-Scale Modelling of Coastal Flooding Due to Tides, Storm Surges and Rivers Inflows. A Cork City Example." *Coastal Engineering* 121(February 2016): 278–96. doi:10.1016/j.coastaleng.2016.12.006.
- 1000 Paprotny, Dominik, Michalis I. Vousdoukas, Oswaldo Morales-Nápoles, Sebastiaan N. Jonkman, and Luc Feyen. 2018. "Compound Flood Potential in Europe." *Hydrology and Earth System Sciences Discussions*: 1–34. doi:https://doi.org/10.5194/hess-2018-132.
- Pont, D., J.W. Day, P. Hensel, E. Franquet, F. Torre, P. Rioual, C. Ibànez, and E. Coulet. 2002. "Response Scenarios for the Deltaic Plain of the Rhône in the Face of an Acceleration in the Rate of Sea-Level Rise with Special Attention to Salicornia-Type Environments." *Estuaries* 25(3): 337–58.
  - Province, The People's Committee of Ca Mau. 2023. Comprehensive Report on Planning for Ca Mau Province during 2021–2030, with a Vision to 2050. Ca Mau Province.
- Ritter, A., and R. Muñoz-carpena. 2013. "Performance Evaluation of Hydrological Models: Statistical Significance for Reducing Subjectivity in Goodness-of-Fit Assessments." *Journal of Hydrology* 480: 33–45. doi:10.1016/j.jhydrol.2012.12.004.
  - Son, Nguyen-thanh, Chi-farn Chen, Ni-bin Chang, Cheng-ru Chen, Ly-yu Chang, and Bui-xuan Thanh. 2015. "Mangrove Mapping and Change Detection in Ca Mau Peninsula, Vietnam, Using Landsat Data and Object-Based Image Analysis." *IEEE Journal of Selected Topics in Applied Earth Observations and Remote Sensing* 8(2): 503–10. doi:10.1109/JSTARS.2014.2360691.
- Sunkur, Reshma, Komali Kantamaneni, Chandradeo Bokhoree, and Shirish Ravan. 2023. "Mangroves' Role in Supporting Ecosystem-Based Techniques to Reduce Disaster Risk and Adapt to Climate Change: A Review." *Journal of Sea Research* 196(October): 102449. doi:10.1016/j.seares.2023.102449.
  - Syvitski, J.P.M., A.J. Kettner, I. Overeem, E.W.H. Hutton, M.T. Hannon, G. R. Brakenridge, J. Day, et al. 2009. "Sinking Deltas Due to Human Activities." *Nature Geoscience* 2: 681–86. doi:10.1038/ngeo629.
- Temmerman, Stijn, Patrick Meire, Tjeerd J. Bouma, Peter M.J. Herman, Tom Ysebaert, and Huib J. De Vriend. 2013. "Ecosystem-Based Coastal Defence in the Face of Global Change." *Nature* 504(7478): 79–83. doi:10.1038/nature12859.
  - Thuy, Linh, My Nguyen, Hanh Thi Hoang, Han Van Ta, and Pil Sun Park. 2020. "Comparison of Mangrove Stand Development on Accretion and Erosion Sites in Ca Mau, Vietnam." *MDPI*: 1–16.
- Thuy, Linh, My Nguyen, Hanh Thi, Eunho Choi, and Pil Sun. 2023. "Estuarine, Coastal and Shelf Science Distribution of Mangroves with Different Aerial Root Morphologies at Accretion and Erosion Sites in Ca Mau Province, Vietnam."

  Estuarine, Coastal and Shelf Science 287(March): 108324. doi:10.1016/j.ecss.2023.108324.

- Tinh, Huynh Quoc, Enrique P Pacardo, Inocencio E Buot, and J Antonio. 2009. "Composition and Structure of the Mangrove Forest at the Protected Zone of Ca Mau Cape National Park, Vietnam." *Journal of Environmental Science and Management* (April 2015).
- Tran, Anh Van, Maria Antonia Brovelli, Khien Trung Ha, Dong Thanh Khuc, Duong Nhat Tran, Hanh Hong Tran, and Nghi Thanh Le. 2024. "Land Subsidence Susceptibility Mapping in Ca Mau Province, Vietnam, Using Boosting Models." 
  ISPRS International Journal of Geo-Information 13(5): 1–24. doi:10.3390/ijgi13050161.
- Tran, Duc Dung, Gerardo Van Halsema, Petra J.G.J. Hellegers, Long Phi Hoang, Tho Quang Tran, Matti Kummu, and Fulco Ludwig. 2018. "Assessing Impacts of Dike Construction on the Flood Dynamics of the Mekong Delta." *Hydrology and Earth System Sciences* 22(3): 1875–96. doi:10.5194/hess-22-1875-2018.
  - Tran, T, VT Nguyen, TLH Huynh, VK Mai, XH Nguyen, and Doan HP. 2016. *Kịch Bản Biến Đổi Khí Hậu và Nước Biển Dâng Cho Việt Nam (Climate Change and Sea Level Rise Scenarios for Vietnam)*. Nhà xuất bản Tài Nguyên Môi Trường và Bản Đồ Việt Nam, Bộ Tài Nguyên và Môi Trường, Hà Nội, p 188 [Publishing House of Natural Resources, Environment and Cartography, Ministry of Natural Resources and Environment, Ha Noi, p 188]. http://www.imh.ac.vn/files/doc/KichbanBDKH/KBBDKH\_2016.pdf.

- Triet, N.V.K., N.V. Dung, H. Fujii, M. Kummu, B. Merz, and H. Apel. 2017. "Has Dyke Development in the Vietnamese Mekong Delta Shifted Flood Hazard Downstream?" *Hydrology and Earth System Sciences Discussions*: 3991–4010. doi:https://doi.org/10.5194/hess-21-3991-2017.
- Triet, Nguyen Van Khanh, Nguyen Viet Dung, Long Phi Hoang, Nguyen Le Duy, Dung Duc Tran, Tran Tuan Anh, Matti Kummu, Bruno Merz, and Heiko Apel. 2020. "Future Projections of Flood Dynamics in the Vietnamese Mekong Delta." *Science of the Total Environment* 742: 140596. doi:10.1016/j.scitotenv.2020.140596.
  - Tu, L. X., V.Q. Thanh, J. Reyns, S.P. Van, D.T. Anh, T.D. Dang, and D. Roelvink. 2019. "Sediment Transport and Morphodynamical Modeling on the Estuaries and Coastal Zone of the Vietnamese Mekong Delta." *Continental Shelf Research*: 64–76. doi:10.1016/j.csr.2019.07.015.
- 1050 Van, P. D.T., I. Popescu, A. Van Griensven, D. P. Solomatine, N. H. Trung, and A. Green. 2012. "A Study of the Climate Change Impacts on Fluvial Flood Propagation in the Vietnamese Mekong Delta." *Hydrology and Earth System Sciences* 16(12): 4637–49. doi:10.5194/hess-16-4637-2012.
- Vasilopoulos, G., Q. L. Quan, D. R. Parsons, S. E. Darby, V. P.D. Tri, N. N. Hung, I. D. Haigh, et al. 2021. "Establishing Sustainable Sediment Budgets Is Critical for Climate-Resilient Mega-Deltas." *Environmental Research Letters* 16. doi:10.1088/1748-9326/ac06fc.
  - Västilä, K., M. Kummu, C. Sangmanee, and S. Chinvanno. 2010. "Modelling Climate Change Impacts on the Flood Pulse in

- the Lower Mekong Floodplains." Journal of Water and Climate Change 1(1): 67–86. doi:10.2166/wcc.2010.008.
- Vu, Hoang Thai Duong, Van Cong Trinh, Dung Duc Tran, Peter Oberle, Stefan Hinz, and Franz Nestmann. 2021. "Evaluating the Impacts of Rice-Based Protection Dykes on Floodwater Dynamics in the Vietnamese Mekong Delta Using Geographical Impact Factor (Gif)." *Water (Switzerland)* 13(9). doi:10.3390/w13091144.
  - Wahl, Thomas, P. Ward, H. Winsemius, Amir AghaKouchak, J. Bender, I. Haigh, S. Jain, et al. 2018. "When Environmental Forces Collide." *Eos Science News by AGU* 99. doi:10.1029/2018eo099745.
  - Ward, P.J., A. Couasnon, D. Eilander, I.D. Haigh, A. Hendry, S. Muis, T.I.E. Veldkamp, H.C. Winsemius, and T. Wahl. 2018. "Dependence between High Sea-Level and High River Discharge Increases Flood Hazard in Global Deltas and Estuaries." *Environmental Research Letters* 13. doi:10.1088/1748-9326/aad400.

- Wood, M., I.D Haigh, Q.Q. Le, H.N. Nguyen, H.B. Tran, S.E. Darby, R. Marsh, et al. 2023. "Climate-Induced Storminess Forces Major Increases in Future Storm Surge Hazard in the South China Sea Region." *Natural Hazards and Earth System Sciences* 23: 2475–2504. doi:https://doi.org/10.5194/nhess-23-2475-2023.
- Zoccarato, Claudia, Philip S.J. Minderhoud, and Pietro Teatini. 2018. "The Role of Sedimentation and Natural Compaction in a Prograding Delta: Insights from the Mega Mekong Delta, Vietnam." *Scientific Reports* 8(1): 1–12. doi:10.1038/s41598-018-29734-7.